Ocean Engineering 240 (2021) 109891

Contents lists available at ScienceDirect

Ocean Engineering

journal homepage: www.elsevier.com/locate/oceaneng

Baseline design of a subsea shuttle tanker system for liquid carbon dioxide transportation

Yucong Ma *, Yihan Xing, Muk Chen Ong, Tor Henning Hemmingsen

Department of Mechanical and Structural Engineering and Materials Science, University of Stavanger, 4036, Stavanger, Norway

ARTICLE INFO

Keywords:
Subsea shuttle tanker
Autonomous underwater vehicle
Carbon capture and storage
CO_2 transportation

ABSTRACT

This paper presents the baseline design of a 34,000-tonne subsea shuttle tanker (SST). The SST is proposed as an alternative to subsea pipelines and surface tankers for the transportation of liquid carbon dioxide (CO_2) from existing offshore/land facilities to marginal subsea fields. In contrast to highly weather-dependent surface tanker operations, the SST can operate in any condition underwater. The SST is an electric-powered autonomous underwater vehicle with a length and beam of 164 m and 17 m, respectively. It has a cargo carrying capacity of 16,362 m^3. This capacity is sufficient to allow the SST to fulfil the annual storage demands of ongoing carbon capture and storage (CCS) projects in Norway. It travels with a slow speed of 6 knots at 70 m constant water depth for maximum energy efficiency and offloads CO_2 via a connected coupling to the subsea well where CO_2 is directly injected. To be economically attractive, the SST has a high payload of 50% displacement which makes a low structural weight design extremely crucial. This is achieved by employing a double hull design for the SST with active pressure compensating systems to cope with the large collapse pressure loads underwater.

1. Introduction

Most offshore oil and gas productions are transported by pipelines from floating production units (FPUs) to onshore facilities (Fullenbaum et al., 2013). Subsea pipeline laying techniques have advanced tremendously since the first pipeline was laid underwater during World War II in the UK and is now considered a mature technology (Palmer and King, 2008). However, this transportation method has some limitations due to technical and economic reasons. One major constraint of the method is the deployment cost which can be exceedingly expensive for remote oil and gas fields due to long transmission lengths since costs increase significantly with pipeline lengths. In addition, deep-water pipeline inspections can be challenging and expensive. Besides, pipeline maintenance and repair frequently require a full line or partial shut-in, which can be economically undesirable. This means the solution is more suitable to large fields with high profit margins and small stepouts (Wilson, 2008), i.e., it is economically unattractive to utilise subsea pipelines to a single remote marginal field. In this situation, shuttle tankers are frequently employed (Vestereng, 2019). The tanker ship is a highly flexible solution which can be deployed on demand to different fields. Further, a replacement tanker can be easily deployed in the event of a vessel down-time. However, being a floating structure that experiences large dynamic load-effects from wind and waves, operation of the tanker ship is highly weather-dependent and cannot be carried out in severe sea states. As an innovative alternative to circumvent the above limitations, the authors present a 34,000-tonne baseline design of a Subsea Shuttle Tanker (SST) (Illustrated in Fig. 1; the engineering drawing is presented in Fig. 7) (Equinor Energy AS, 2019; Ellingsen et al., 2020; Xing et al., 2021) which combines the flexibility and economy of the shuttle tanker together with the ability of the submarine to operate in any weather conditions underwater.

The idea of using underwater vehicles in commercial transportation is not new and was earlier proposed in the 1970s where Jacobsen (1971) and Taylor et al. (1977) proposed the use of nuclear propelled submarines of various sizes (20,000 to 420,000 DWT) for the transportation of Arctic crude oil. Moving forward to the 1980s, Jacobsen et al. (1983) proposed two mammoth submarine Arctic LNG tanker concepts: a 660, 800 DWT nuclear-powered and a 727,400 DWT non-nuclear-powered version. More recently, Brandt et al. (2015) presented a 3500 DWT multi-purpose submarine for a wide range of subsea operations including installation, inspection, maintenance and repair up to water depths of 1500 m in the Arctic region. An innovative maritime freight option was also presented by Ellingsen et al. (2020) in which a subsea 'cargo-train' made up of inter-connected subsea train-like tanks with

* Corresponding author.
E-mail address: yucong.ma@uis.no (Y. Ma).

https://doi.org/10.1016/j.oceaneng.2021.109891
Received 9 July 2021; Received in revised form 3 September 2021; Accepted 17 September 2021
Available online 26 October 2021

independent propulsion units located at the vessel bow or aft was proposed. Ellingsen et al. (2020) also proposed an ultra-efficient large subsea transport glider. This subsea glider was envisioned to have large hydrodynamic wings with the cargo tanks mounted within. Xing (2021) went on to propose a 1500 DWT subsea cargo glider that has a calculated average power consumption of below 10 kW. In general, the above-mentioned works did not go beyond conceptual design proposals. In this paper, the authors will close this knowledge gap by defining a baseline SST design that entails detailed global design specifications. The paper will build upon the background work performed in Xing et al. (2021) where the most important design considerations surrounding the global weight distribution, structural capacity, cargo properties, pressure compensation system and offloading methods were investigated.

The main objective of the SST is to transport CO_2 from offshore or land facilities to subsea wells for direct injection by travelling autonomously underwater. Its position in the offshore carbon capture and storage (CCS) supply chain operations is illustrated in Fig. 2. The baseline SST is defined for deployment in the Norwegian sector where there are currently three ongoing CCS projects, namely Sleipner, Utgard, and Snøhvit (Norwegian Petroleum Directorate (NPD), 2020). In these projects, CO_2 generated from hydrocarbon production is captured and reinjected into the reservoir. In addition to these three ongoing projects, the Northern Lights project (Equinor ASA, 2020) will start operation in 2024 where CO_2 generated from land-based, non-petroleum related industrial activities will be transported to the Troll field for injection into the Utsira formation. The locations of the above-mentioned CCS projects are shown in Fig. 3. These Norwegian fields are selected to provide the mission requirements as they are already being exploited for CCS storage. The SST can be designed to operate in different sites around the world that may have different requirements. Even though the target cargo is CO_2, the SST can be also used to transport other types of cargo such as hydrocarbons, electrical power (through batteries), and subsea tools.

The SST can contribute to the mitigation of global warming in different ways. On one side, it is fully electrically powered and emission-free which contributes to the sustainability of shipping. Shipping currently accounts for approximately 3.3% of fossil-fuel-related CO_2 emissions (Papanikolaou, 2014). On the other side, it enables marginal subsea fields to be utilised as offshore CO_2 storage sites, thereby supporting to meet the future increasing global demand in CCS. The majority of CO_2 released by industrial activities can be captured and stored (Capture and Storage Association (CCSA), 2020). Any economical solution that can increase the global CCS storage supply is crucial to moderate the exaggerating trend in the increase of global mean temperature. This is likely to be worsen by the increasing trend in global energy demand which will cause the atmospheric CO_2 concentration to double in 2100 compared to 1960 levels (International Energy Agency (IEA), 2010).

2. Design methodology

The design methodology used is presented in Fig. 4 as a design flowchart and is briefly discussed in this section. The design of SST starts from the mission requirements (Ref. Section 3), in which the depth, range, cargo capacity, and environmental data are identified. The mission requirements will consequently define the properties of the CO_2 cargo (Ref. Section 4), expected load-effects, required speed, and range.

The expected load-effects will define the structural properties (Ref. Section 7) and these are results of the loads experienced due to water depth, offloading (Ref. Section 10) and CO_2 cargo. In structural properties (Ref. Section 7), the external hull, inner tank, and materials used are defined. At the same time, a pressure compensation system (PCS) (Ref. Section 9) is also proposed to mitigate large collapse pressure loads. The PCS is a design innovation specific to the SST and is used under all types of mission requirements.

The required speed and range will define the hydrodynamics and propulsion design (Ref. Section 8). These are also affected by manoeuvrability and the resulting external hull geometry defined from the structural properties. Drag and power, propeller design, energy consumption and battery selection are defined in Section 8.

Finally, the hydrostatic properties (Ref. Section 6) are calculated based on the general arrangement and component weights (Ref. Section 5) defined from above and checked against the stability criterion. Both transverse and longitudinal hydrostatic stabilities are checked. The

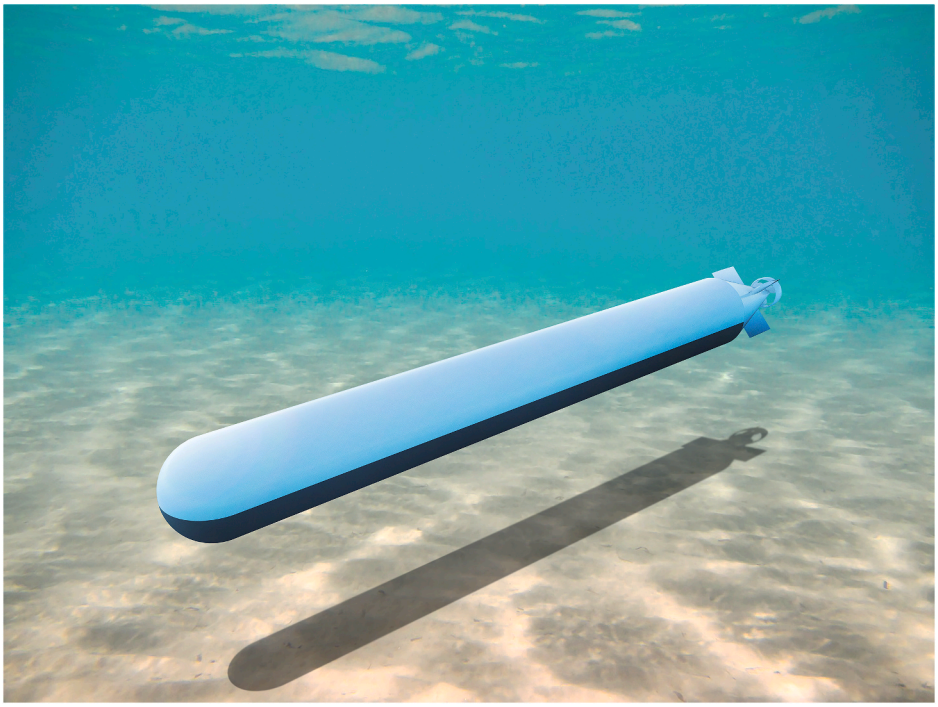

Fig. 1. Illustration of the subsea shuttle tanker.

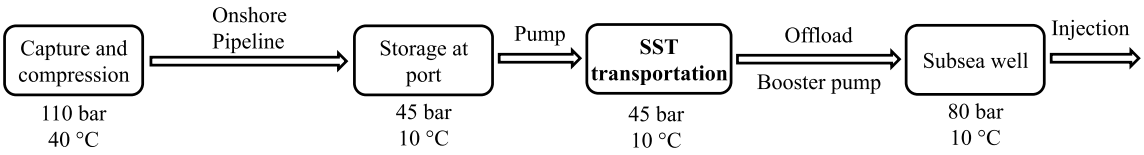

Fig. 2. CCS offshore storage process with SST transportation.

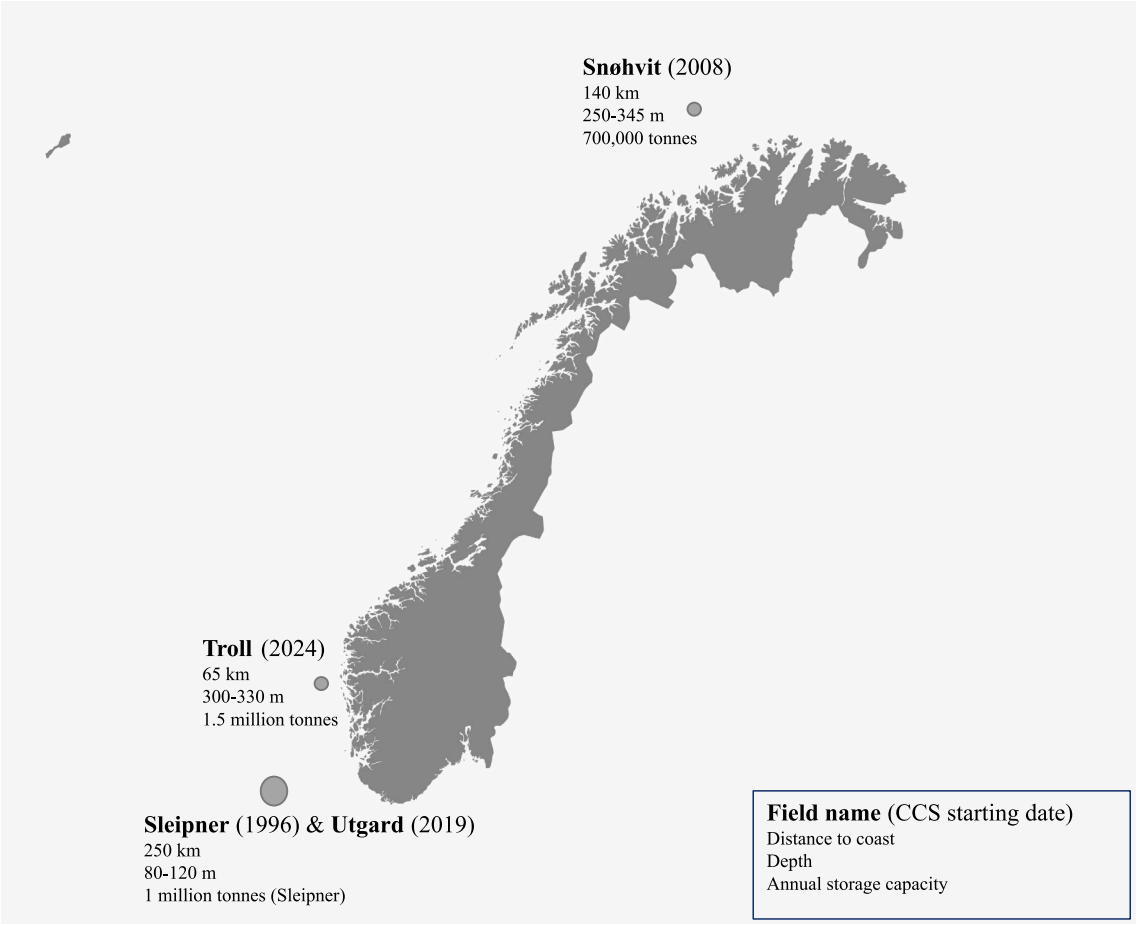

Fig. 3. Current ongoing and planned CCS storage sites in the Norwegian sector (data from Norwegian Petroleum Directorate (NPD) (2020) and Equinor ASA (2020)).

baseline design is obtained if the stability criterion is fulfilled; otherwise, the structural properties will be adjusted, and the design will be iterated. The resulting main parameters of the baseline design are presented in Table 1. Using the design procedure, the SST derived is a 33,619-ton submarine with a length and beam of 164 and 17 m, respectively. It can carry up to 16,362 m^3 of CO_2 for a range of up to 400 km at a speed of 6 knots.

The subsequent sections will discuss individual aspects of the baseline design in more details.

3. Mission requirements

The mission requirements set the premise of the design and are defined and discussed in this section.

3.1. Operating depth range

The SST has the following depth definitions:

- The safety depth is 40 m.
  - This is to avoid collisions with draught surface ships or floating installations.
- The nominal diving depth is 70 m.
  - The SST is designed to travel at a constant 70 m nominal diving depth. This depth is defined based on the minimum recoverable depth from lost-of-control situations, e.g., jam-to-rise. The determination process of the nominal diving depth is given in Appendix A.
- The test diving depth is 105 m.
  - The test diving depth of the SST is 105 m which is defined to be 1.5 times of the nominal diving depth in accordance with DNVGL-RU-NAVAL-Pt4Ch1, Table 1 (DNV-GL, 2018).
- The collapse depth is 190 m.
  - The SST is designed not to collapse at maximum 190 m depth which is defined to be 2.7 times of the nominal diving depth in accordance with DNVGL-RU-NAVAL-Pt4Ch1, Table 1 (DNV-GL, 2018).

Based on the above depth definitions, the operating depth range of the SST is therefore between 40 m (safety depth) and 70 m (nominal diving depth). Emergency procedures using the PCS will be initiated

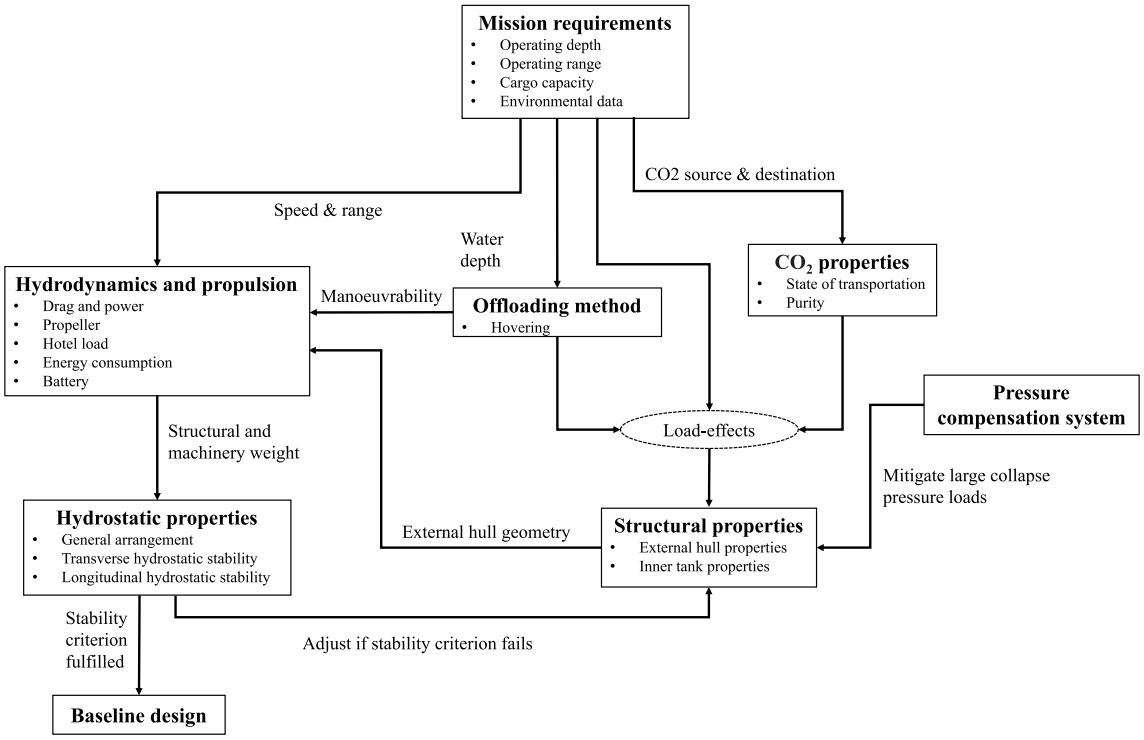

Fig. 4. Design flow chart used in SST baseline design.

Table 1
Subsea shuttle tank main design parameters.

Parameter	Value	Unit
Length	166	[m]
Beam	17	[m]
Displacement	33,619	[tonnes]
Collapse depth	190	[m]
Operating depth	70	[m]
Operating speed	6	[knots]
Maximum range	400	[km]
Cargo volume	16,362	[m^3]
Current speed	1	[m/s]
Cargo pressure	35–55	[bar]
Cargo temperature	0–20	[C]

when the hydrostatic pressure exceeds the tank pressure to prevent cargo tank failure. These procedures are presented in Section 9. The definition of the depths is illustrated in Fig. 5 together with the depths of the CCS storage sites considered in this paper.

3.2. Range

The SST's range is designed to be 400 km which will enable it to make a return trip to Snøhvit and Troll or a one-way trip to Sleipner and Utgard. In the latter case, the SST can be recharged using the existing offshore facilities at the Utsira High, which is electrified from shore.

3.3. Cargo capacity

The SST's cargo capacity is designed to be 15,000 tonnes to match the maximum annual carbon storage capacity of the CCS projects considered in this paper which is 1.5 million tonnes as presented in Fig. 3. This can be fulfilled using two weekly scheduled SST trips.

3.4. Environmental data

The following environmental conditions are defined:

- The design minimum and maximum environmental temperatures are 0 °C and 20 °C, respectively.
  - The SST will operate in the Norwegian Sea (0 °E – 10 °E, 60 °N - 70 °N). In this region, the seawater temperature range is 2 °C–12 °C (NCEI, 2020). The minimum of 0 °C is have a slight temperature margin during winters; the temperatures in sea water normally do not go below 0 °C. The maximum of 20 °C is to cover the case where SST surfaces during summers.
- The design seawater density is 1025 kg/m^3.
  - This is the corresponding minimum seawater density based on the seawater temperatures presented above. A minimum density value will lead a lower buoyancy force being used in neutral-buoyancy design calculations. This is conservative as an insufficient buoyancy force appearing at the later stages of the design or construction process could mean increasing the length of the vessel, which is a very costly exercise.
- The design current speed is 1 m/s.
  - In the Norwegian Sea, the observed seasonal average current speed is around 0.2 m/s while the highest seasonal average speed is around 1 m/s of the North Atlantic Current and Norwegian coastal current (Mariano et al., 1995; Ersdal, 2001; Sætre, 2007).

4. CO_2 properties

4.1. State of transportation

CO_2 is normally transported offshore in the supercritical state and saturated liquid state using pipelines and ships, respectively. The SST transports CO_2 in the saturated liquid state with pressure and temperature of 35–55 bar and 0–20 °C, respectively. In the saturated liquid state, the temperature and pressure are passively regulated with the environment, i.e., no external energy is required to maintain them at the defined set points. This means the pressure of the liquid CO_2 will vary along the boiling line in the phase diagram (Fig. 6) during transportation. This is an energy-effective and therefore cost-effective solution. This transport method contrasts with existing gas carriers which

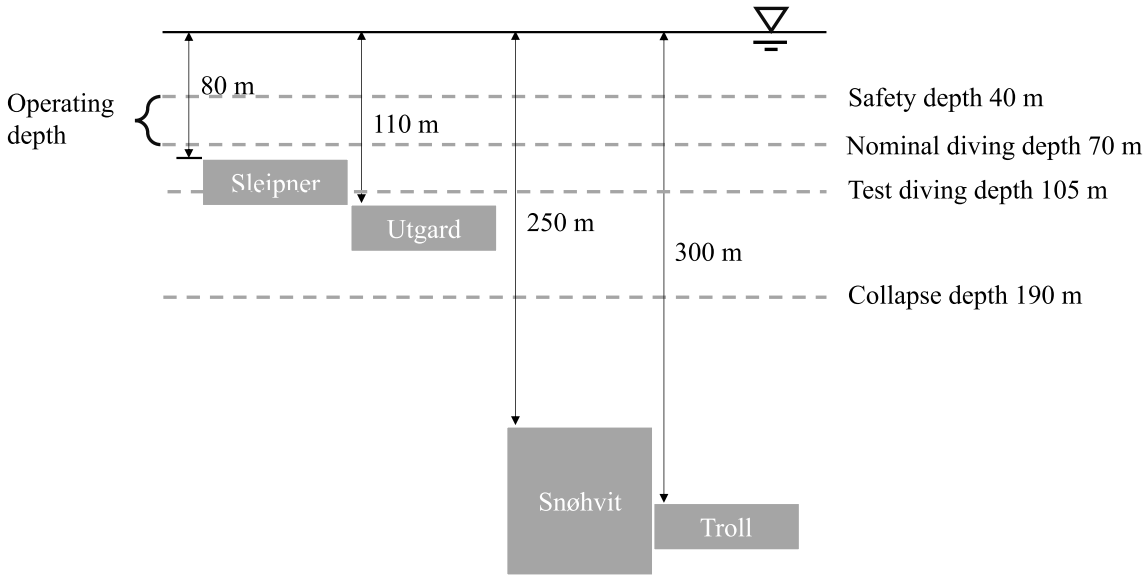

Fig. 5. Depth definitions together with depths of CCS storage sites considered.

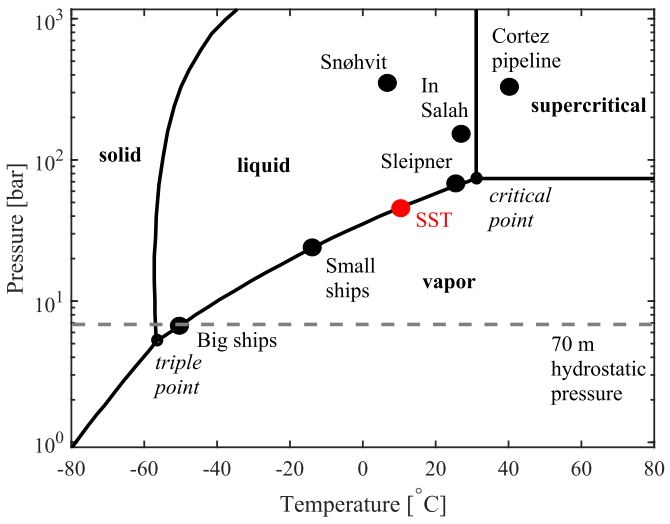

Fig. 6. CO_2 phase diagram presented together with the CO_2 states associated with various transportation methods and wellhead injection conditions from Equinor ASA (2021) and Eiken et al. (2011).

are commonly the semi-refrigerated (small ships) and refrigerated (large ships) types. These carriers require re-liquefaction systems which are both cost- and energy-intensive to run. For example, these big and small ships must maintain low temperatures of −50 °C and −15 °C, respectively as shown in Fig. 6. To maintain these low temperatures, re-liquefaction systems with compressors are needed to capture the boil-off gas. By transporting saturated liquid CO_2 at environmental temperature, the use of these energy-intensive systems for the SST is avoided.

Moreover, the liquid CO_2 at 45 bar can be directly pumped using a single stage booster pump into the reservoir (wellhead pressures are about 80 bar in Sleipner & Utgard). This is significantly more efficient compared to gas carriers where multi-stage booster pumps and inter-heaters are required. For instance, small CO_2 carriers need to increase the pressure of the liquid from 8 bar to 80 bar and the temperature from −15 °C to 25 °C.

4.2. Purity

CO_2 quality or purity is important to the SST's structural design because impurities increase the risk for corrosion and hydrate formation. As discussed in Xing et al. (2021), the most undesired impurity for the SST is free water (H_2O). Free water dissolves CO_2 and H_2S to form the highly corrosive carbonic and sulphuric acids; the latter is formed together with oxygen (De Visser et al., 2008 and Mohitpour et al., 2007). These acids can lead to severe corrosion issues in the SST. On the other hand, hydrate formation in the cargo tanks can cause blockage and/or sealing issues. This is particularly relevant for the seals in the pistons of the PCS (Ref. Section 9). Free water is avoided in the SST by ensuring that the water concentration is always lower than its solubility, i.e., there will be no free water if all the water dissolves in CO_2. The baseline design uses the impurity limits from the Northern Lights project (Equinor ASA, 2021) as the SST is designed to operate in the Norwegian sector. The impurities limits are presented in Table 2 together with the limits from the Dynamis project (Bonis, 2012) as reference. The free water limit is defined to be 30 ppm which is much lower than the lowest solubilities of H_2O presented in Xing et al. (2021); 200 ppm and 1200 ppm considering CO_2 gas and liquid at −10 °C, respectively. This ensures that no free water will be present in the CO_2 cargo. It is mentioned that limits are placed on nitrogen oxides (NO_x), sulphur oxides (SO_x) and hydrogen sulphide (H_2S) in Northern Lights and Dynamis due to safety and health considerations. These may not be mandatory for the SST since the vessel is unmanned.

5. General arrangement

5.1. Compartments

The general arrangement is presented in Fig. 7. As shown in the figure, two watertight bulkheads divide the SST into three compartments:

- Free flooding aft compartment: Contains the moisture-sensitive equipment that includes the motor, gearbox, rudder controls, battery, aft trim tank, and aft compensation tank.

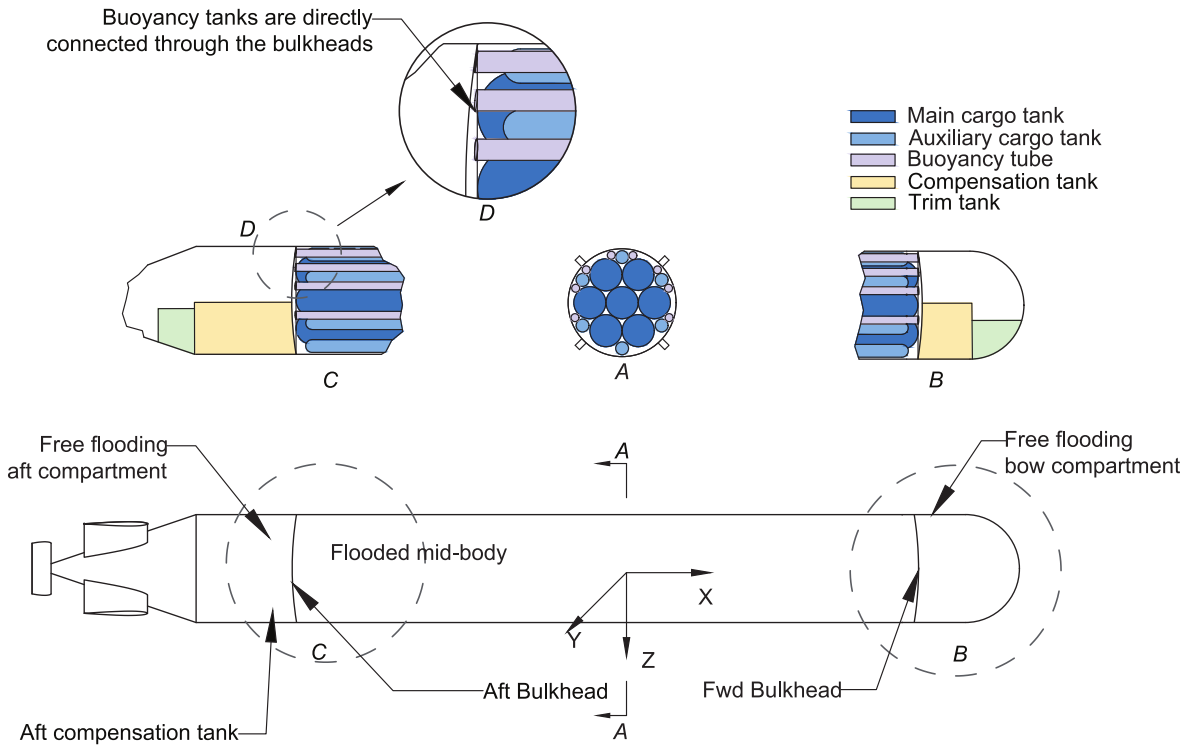

Fig. 7. SST general arrangement. A: Mid-vessel cross section. B: SST fwd bulkhead. C: SST aft bulkhead. D: Buoyancy tank-bulkhead connection.

Table 2
CO_2 impurity limits. Limits from the Northern Lights project (Equinor ASA, 2021) are used. Limits from the Dynamis project (Bonis, 2012) are provided as reference.

Component	SST allowable	Northern Lights	Dynamis
Water, H_2O	30 ppm		500 ppm
Sulphur oxides, SO_x	10 ppm		100 ppm
Nitrogen oxides, NO_x	10 ppm		100 ppm
Hydrogen sulphide, H_xS	9 ppm		200 ppm
Carbon monoxide, CO	100 ppm		200 ppm
Oxygen, O_2	10 ppm		non-considerable gases < 40,000 ppm
Amines, RNH_3	10 ppm		non-considerable gases < 40,000 ppm
Ammonia, NH_3	10 ppm		non-considerable gases < 40,000 ppm
Hydrogen, H_2	50 ppm		non-considerable gases < 40,000 ppm
Formaldehyde, HCHO	20 ppm		non-considerable gases < 40,000 ppm
Acetaldehyde, CH_3CHO	20 ppm		non-considerable gases < 40,000 ppm

- Free flooding bow compartment: Contains the sensors, sonar, radio, control station, pumps for offloading, fwd trim tank, and fwd compensation tank.
- Flooded mid-body: The largest compartment and contains the buoyancy tanks, cargo tanks, and piping.

Table 3
Dry weight and volume distribution. Tank arrangement and positions can be found in Figs. 7 and 8.

Component	CoG (x, y, z) [m]	Weight [ton]	Space [m^3]
External hull	(-7.1, 0.0,0.0)	2666	32,799
Main cargo tank 1	(0.0, 0.0, 0.0)	681	1931
Main cargo tank 2	(0.0, 5.0, 0.0)	681	1931
Main cargo tank 3	(0.0, 2.5, 4.3)	681	1931
Main cargo tank 4	(0.0, −2.5, 4.3)	681	1931
Main cargo tank 5	(0.0, −5.0, 0.0)	681	1931
Main cargo tank 6	(0.0, −2.5, −4.3)	681	1931
Main cargo tank 7	(0.0, 2.5, −4.3)	681	1931
Auxi. Cargo tank 1	(0.0, −7.1, 0.0)	171	475
Auxi. Cargo tank 2	(0.0, 6.2, −3.6)	171	475
Auxi. Cargo tank 3	(0.0, 6.2, 3.6)	171	475
Auxi. Cargo tank 4	(0.0, 7.1, 0.0)	171	475
Auxi. Cargo tank 5	(0.0, −6.2, 3.6)	171	475
Auxi. Cargo tank 6	(0.0, −6.2, −3.6)	171	475
Buoyancy tank 1	(0.0, −7.5, 2.1)	46	123
Buoyancy tank 2	(0.0, −7.5, −2.1)	46	123
Buoyancy tank 3	(0.0, −5.6, −5.4)	46	123
Buoyancy tank 4	(0.0, −1.9, −7.5)	46	123
Buoyancy tank 5	(0.0, 1.9, −7.5)	46	123
Buoyancy tank 6	(0.0, 5.6, −5.4)	46	123
Buoyancy tank 7	(0.0, 7.5, −2.1)	46	123
Buoyancy tank 8	(0.0, 7.5, 2.1)	46	123
Fwd comp. tank	(65.3, 0.0, 5.0)	100	800
Aft comp. tank	(-65.3, 0.0, 5.0)	100	800
Fwd trim tank	(67.8, 0.0, 5.0)	35	200
Aft trim tank	(-67.8, 0.0, 5.0)	35	200
Fwd bulkhead (watertight)	(50.0, 0.0, 0.0)	147	–
Aft bulkhead (watertight)	(-50.0, 0.0, 0.0)	147	–
Mid-body bulkhead 1	(25.0, 0.0, 0.0)	10	–
Mid-body bulkhead 2	(25.0, 0.0, 0.0)	10	–
Machinery	(-33.7, 0.0, 6.0)	1000	8288
Permanent ballast	(4, 0.0, 8.0)	997	–
Sum	(-4.6, 0.0, 0.9)	11,200	32,799

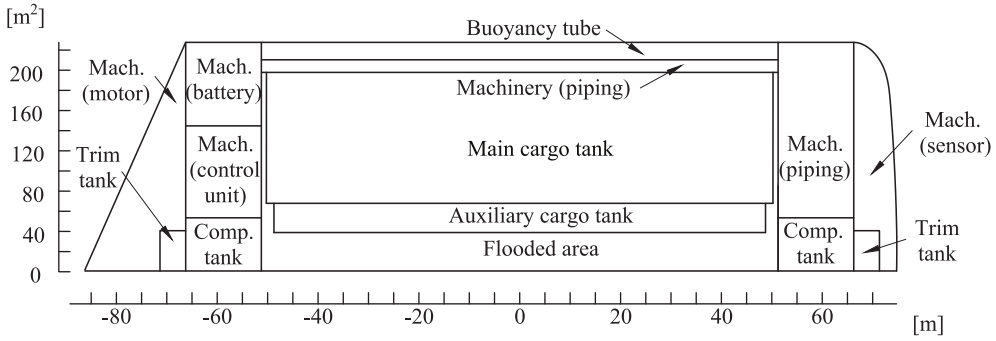

Fig. 8. SST Flounder diagram. Lateral axis: SST longitudinal position; vertical axis: Cross section area.

5.2. Distribution of weights and spaces

Table 3 lists the weights, volumes, and centres of gravity of the SST's major components. The origin of the coordinate system is set at the centroid of the cylindrical mid-body. The Flounder diagram is presented in Fig. 8 and is used to check the disposition of volumes presented in Table 3. It describes the space distribution of the SST along the vessel length without considering the exact layout. The lateral axis represents the longitudinal position of the SST while the vertical axis demarcates the cross-section area. Each individual area in the diagram represents the space demand of each volume component and illustrates the corresponding SST space is used. The weight estimation of the external hull, buoyancy tubes, and cargo tanks are presented in Section 7. The definition of compensation tanks, trim tanks, permanent ballast, and machinery are given as following:

- Compensation tanks: Two 800.0 m^3 compensation tanks are arranged on the SST. Compensation tanks provide the vessel with the trimming moment and weight necessary to reach neutral buoyancy under different hydrostatic load cases. They communicate directly with the open sea using pumps. These tanks can ensure the neutral buoyancy of the SST during all design hydrostatic load cases with a sufficient margin (Ref. Fig. 10 and Section 6.4). The capacity of compensation tanks is determined in accordance with Burcher and Rydill (1994) to be *1.1 × (largest possible weight change + largest possible buoyancy change due to various water density)*.
- Trim tanks: In the SST, two 200.0 m^3 trim tanks locate in the bow hemisphere and aft cone. These tanks bring the centre of gravity (CoG) vertically beneath the centre of buoyancy (CoB) so that the vessel is at a neutral trim condition. The trim tanks do this by pumping water between each other. Trim tanks do not communicate with open sea and are half-filled with water. The sufficiency of trim tanks to cope with the possible change of the SST's longitudinal CoG is proved in Section 6.4.
- Permanent ballast: Permanent ballast is used (i) to assist in achieving neutral buoyancy as a design margin, (ii) to equalise the longitudinal position of CoG and CoB to reach neutral trim, and (iii) to lower the vertical position of CoG to increase hydrostatic stability. The permanent ballast weight is estimated to be 4% of the SST's dry weight corresponds to 997 tonnes. This is close to the design target in Xing et al. (2021).
- Machinery: By engineering judgement, the authors estimate the machinery to be 1000 tonnes. The main components include the moisture-sensitive equipment and piping. For comparison, the USS Albacore has a similar power level (2 MW) with the SST (0.5 MW–1

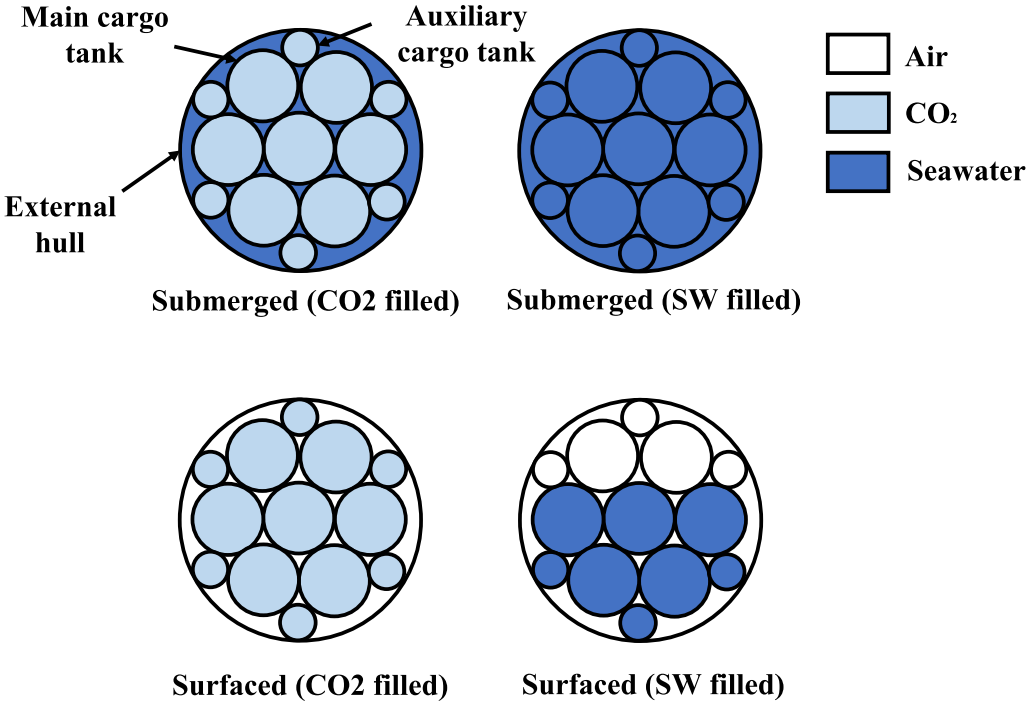

Fig. 9. Mid-vessel cross-sectional views of liquid distributions for various hydrostatic load cases.

MW) and its machinery weight is 638 tonnes (Burcher and Rydill, 1994).

6. Hydrostatics

6.1. Hydrostatic load cases

Hydrostatic stability of the SST is checked against DNVGL-RU-NAVAL-Pt4Ch1, Section 3.5.2.3 (DNV-GL, 2018) which states that the distance between the centres of buoyancy and gravity (BG) and metacentric height (GM) must be greater than 0.35 m in the submerged condition for vessels that exceed 2000 DWT. Further, the metacentric height (GM) must be greater than 0.22 m in the surfaced condition.

The hydrostatic load cases are illustrated in Fig. 9 and described in detail as follows:

- **Submerged (CO2 filled):** The vessel is submerged with all 13 tanks filled with liquid CO_2. The mid-body flooding area is filled with seawater. The compensation tanks are used to ensure neutral buoyancy. This is the fully loaded operating conditions.
- **Submerged (SW filled):** The vessel is submerged with all 13 tanks filled with seawater. The mid-body flooding area is filled with seawater ballast. The compensation tanks are empty. This situation occurs after the SST has offloaded at a subsea well.
- **Surfaced (CO2 filled):** The vessel is floating on the surface with all 13 tanks filled with liquid CO_2. The mid-body flooding area is not filled with seawater. The compensation tanks are empty. This situation occurs when the SST is loading at the port.
- **Surfaced (SW filled):** The vessel is floating on the surface with 5 main tanks and 3 auxiliary tanks at the bottom filled with seawater ballast, the remaining tanks are empty. The mid-body flooding area is not filled with seawater. The compensation tanks are empty. This situation occurs when the SST returns to the port after its journey.

6.2. Metacentres and centres of buoyancy & gravity

The metacentre (M), centre of buoyancy (CoB), and centre of gravity (CoG) of the SST for different hydrostatic load cases are listed in Table 4. These values of these parameters affect the hydrostatic stability which is defined by BG and GM when the SST is submerged and floating, respectively. The lowest BG and GM values are 0.57 m and 0.50 m and correspond to the submerged (SW filled) and surfaced (CO2 filled), respectively. These meet the criteria of 0.35 m and 0.22 m listed in DNVGL-RU-NAVAL-Pt4Ch1, Section 3.5.2.3 (DNV-GL, 2018), respectively.

6.3. Weight and space composition

The weight and space composition with respect to the design hydrostatic load cases are listed in Table 5. The SST dry weight composition is given in Table 6. The double hull design and pure electric propulsion system reduces the structural weight and machinery weight which takes up 35% and 3% of the dry weight, respectively. Consequently, a high payload capacity of 46% of its displacement and 50% of its volume is achieved.

6.4. Equilibrium polygon plot

During CO_2 offloading, seawater is pumped in from one side of the cargo tank thereby pushing the piston of the PCS system (Section 9) and consequently the CO_2 from the other end of the tank. This means the cargo tanks will go from a state of being (i) fully CO_2 filled to (ii) partially CO_2 and seawater filled and finally to (iii) fully seawater filled. This affects the longitudinal CoG positions and individual weights of the cargo tanks as CO_2 and seawater have different densities, 940 vs 1025 kg/m^3, respectively. As a result, the global SST's longitudinal stability and weight are consequently affected. Eight cargo tank loading conditions are investigated, and these are presented in Table 7 and plotted together with an equilibrium polygon in Fig. 10. The equilibrium polygon indicates the maximum compensating ballast weight and trimming moment that can be achieved by the compensation tanks and trim tanks. All load cases considered lie within the polygon which means the SST is longitudinally stable, i.e., sufficient trimming moments can be generated to maintain longitudinal stability in all conditions. Further,

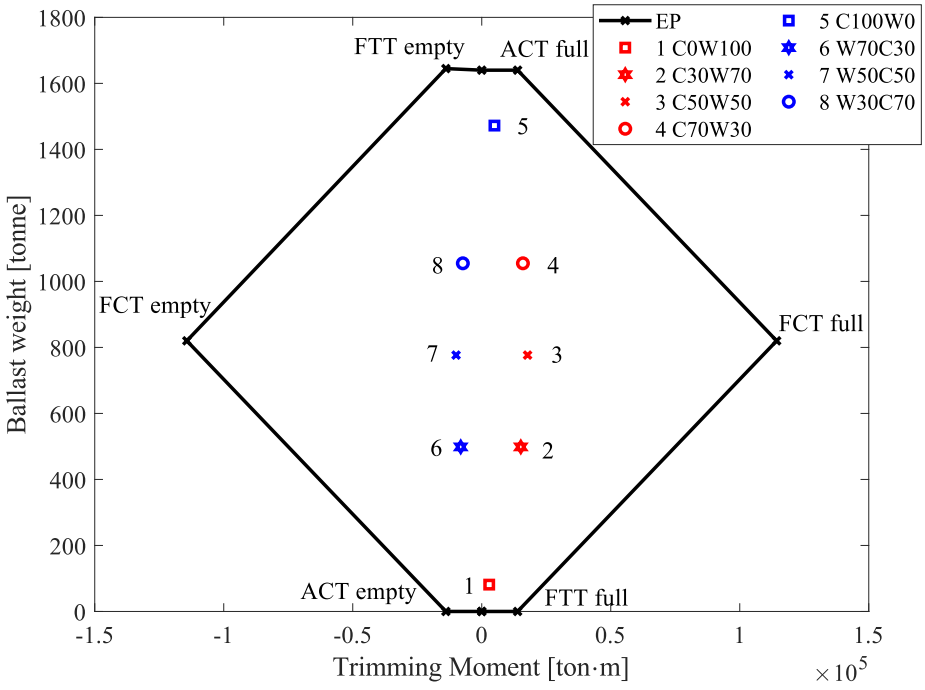

Fig. 10. Equilibrium polygon of the SST with load cases specified in Table 7. EP: equilibrium polygon, LC: loading condition, FTT: fwd trim tank, FCT: fwd compensation tank, ATT: aft trim tank, ACT: aft compensation tank.

Table 4
Centres of the SST and hydrostatic check (units = m).

	Submerged (CO2 filled)	Submerged (SW filled)	Surfaced (CO2 filled)	Surfaced (SW filled)
CoB (x, y, z)	(-1.43, 0.00, 0.00)	(-1.43, 0.00, 0.00)	(-1.75,0.00,1.36)	(-1.78, 0.00, 2.18)
CoG (x, y, z)	(-1.43, 0.00, 0.78)	(-1.43, 0.00, 0.57)	(-1.75, 0.00, 0.50)	(-1.78, 0.00, 1.35)
M (x, y, z)	(0.00,0.00,0.00)	(0.00,0.00,0.00)	(0.00,0.00,0.00)	(0.00,0.00,0.00)
GM	0.78	0.57	0.50	1.35
BG	0.78	0.57	−0.86	−0.83
Result	BG > 0.35 = = OK	BG > 0.35 = = OK	GM > 0.22 = = OK	GM > 0.22 = = OK

Table 5
Weight and space composition.

Component	Weight (tonnes)				Space [m^3]
	Submerged (CO2 filled)	Submerged (SW filled)	Surfaced (CO2 filled)	Surfaced (SW filled)	
Cargo tank	15,381 (46%)	16,772 (49%)	15,381 (57%)	11,354 (50%)	16,362 (50%)
Structure	9413 (28%)	9413 (28%)	9413 (35%)	9413 (41%)	1169 (4%)
Machinery	1000 (3%)	1000 (3%)	1000 (4%)	1000 (4%)	8288 (26%)
Mid-body seawater	5152 (15%)	5152 (15%)	0 (0%)	0 (0%)	5027 (15%)
Compensation ballast	1469 (4%)	79 (0.2%)	0 (0%)	0 (0%)	1600 (4%)
Trim ballast	205 (1%)	205 (1%)	205 (1%)	205 (1%)	400 (1%)
Permanent ballast	997 (3%)	997 (3%)	997 (4%)	997 (4%)	–
Sum	33,619 (100%)	33,619 (100%)	26,996 (100%)	22,969 (100%)	32,799 (100%)

Table 6
SST dry weight composition.

Component	SST [tonnes]	SST [% dry weight]
Payload	15,381	57
Structure	9413	35
Machinery	1000	4
Permanent ballast	997	4
Total dry weight	26,791	100

Table 7
Cargo tank loading conditions considered in hydrostatic longitudinal stability check. % is the percentage of cargo tank volume.

Cargo tank loading condition	Liquid in the forward side of the tank	Liquid in the aft side of the tank
C0W100	100% SW	–
C30W70	30% CO_2	70% SW
C50W50	50% CO_2	50% SW
C70W30	70% CO_2	30% SW
C100W0	100% CO_2	–
W70C30	70% SW	30% CO_2
W50C50	50% SW	50% CO_2
W30C70	30% SW	70% CO_2

the x and y values of each point shows the required trimming moment to reach neutral trim and the required ballast to reach neutral buoyancy, respectively. The largest trimming moment occurs when the SST has 50% offloaded and the biggest weight change occurs when the SST is 100% offloaded.

7. Structural properties

7.1. External hull structures

7.1.1. Slenderness ratio

The geometrical properties of the external hull are listed in Table 8 and briefly discussed in this sub-section. The SST uses a torpedo-shaped hull which consists of a hemispherical bow, a 130.5 m long cylindrical mid-body section and a 25 m long conical aft. The diameter is 17 m. The torpedo shape is chosen for its simple geometry and low drag resistance. The geometry is relatively simple as the long cylindrical mid-body section has only curvatures in one direction and can be fabricated using steel plates bent in a single direction; doubly bent plates are in general more complicated to be fabricated accurately. Note that the hemispherical bow and conical aft do have curvatures in two directions and would require plates bent in two directions. The bow and aft portions are only 23% of the total steel external hull weight and are necessary to obtain low drag resistance. It is also mentioned that another advantage of the cylindrical mid-body section is that cargo tanks which are also cylindrical can be efficiently arranged inside to maximise cargo capacity.

Table 8
SST external hull properties.

Parameter	Free flooding bow compartment	Flooded mid-body	Free flooding aft compartment
Length [m]	23.75	100.0	40.25
Thickness [m]	0.041	0.025	0.041
Frame spacing [m]	1.0	1.5	1.0
Steel weight [ton]	521	1374	771
Material type	VL D47	VL D47	VL D47
Yield strength [MPa]	460	460	460
Tensile strength [MPa]	550	550	550
Design collapse pressure [bar]	20	7	20

The slenderness ratio of the vessel is chosen to be 9.7 which gives a drag resistance value that is very close to the theoretical minimum; about 5% more than the minimum value which is associated with the slenderness value of 5.7. This can be observed from the plot of total resistance against slenderness ratio presented in Fig. 11. Details of the calculations used to generate this plot are presented in Appendix B.

7.1.2. External hull properties

The design of large submarines to mitigate against collapse in deep waters is particularly challenging. It is extremely costly to increase the collapse capacity of large diameter, thin-walled structures (Xing et al., 2021). The collapse failure resistance of large diameter, thin-walled structures is very sensitive to geometric imperfections and these imperfections are very difficult to control for large structures where steel plates and beams are typically welded together. For large structures, a 1% imperfection in the diameter can lead to a 50% reduction in the collapse pressure capacity (Ross, 2011). As such, large military

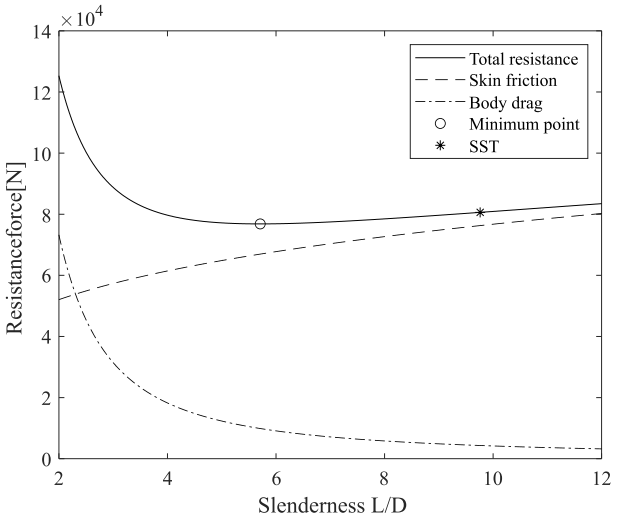

Fig. 11. Resistance force vs slenderness ratio of SST (displacement is fixed while slenderness ratio is varied).

submarines such as Typhoon typically employ heavy and closely space ring-stiffened structures together with high strength steels in their external hulls to achieve the required collapse capacities in deep waters (Šabalja et al., 2014). This typically results in less than 10% displacement available to carry payload, which is undesirable in the SST as it is a cargo transport vehicle (Xing et al., 2021). A weight-optimal structural design is crucial as structures account for around a significant portion of displacement, e.g., can be as much as 40–50% for the case of a military submarine. The SST structural weight should be reduced to around 30% dry weight in order to be economically attractive (Xing et al., 2021). Further, any structural weight that is reduced via optimisation contributes directly to increasing the payload.

In the baseline design, a double hull design is utilised at the cylindrical mid-body to avoid the need for collapse pressure design, i.e., the mid-body is flooded as illustrated in Fig. 12. This means that the mid-body external hull would not experience any hydrostatic pressure differential loading, i.e., the internal and external pressures on the external hull cancel each other. The flooded mid-body external hull is therefore non-pressure loading while the smaller internal pressure hulls, i.e., cargo tanks and buoyancy tubes are designed to handle both burst and collapse pressures. The mid-body is the largest part of the external hull and accounts for 54% of the external hull structural weight. This means a significant amount of weight can be saved if it is not required to handle external pressure; as mentioned above, collapse pressure design is expensive for large structures. The hemispherical bow and conical aft are free flooding compartments and they are checked for the following conditions: nominal diving pressure (7 bar), test diving pressure (10.5 bar), and collapse diving depth (19 bar) in Appendix C. These compartments will also house the machinery and auxiliary equipment which are discussed further in Section 5. All three compartments employ stiffeners to increase the structural and buckling (both global and local) capacities.

VL D47 from DNVGL-RU-SHIP Pt.2 Ch.2 (DNV-GL, 2019) is used as the steel material for all three compartments. VL D47 is a steel material with a high yield and tensile strength of 460 MPa and 550 MPa, respectively. It has good weldability and formability which are essential in the fabrication of cost-efficient but high-quality large steel constructions. It is widely used on large container ship hull structures and can be manufactured by most steel mills, i.e., JFE Steel (2021).

Based on the above definitions, the final structural geometries are calculated using the design calculation method employed from DNVGL-RU-NAVAL-Pt4Ch1, Appendix A, Section 6 (DNV-GL, 2018). The cylindrical mid-section employs 25 mm thick steel plates. The hemispherical bow and conical aft employs 40 mm thick steel plates. Stiffeners with 0.1 m flange widths and 0.3 m web heights are applied to all compartments. The final external hull properties are presented in Table 8. Details of the design calculations are presented in Appendix C.

7.1.3. *Bulkhead properties*

The SST has four bulkheads to separate the flooded mid-body from free flooding compartments and provide support to internal cargo tanks and buoyancy tubes. They are two watertight bulkheads which are located at the forward and aft vessel and two non-watertight bulkheads which are located at the flooded mid-body. The interval between bulkheads is set to be 25 m which corresponds to two hull diameters. This is a common practice for submarines according to Burcher and Rydill (1994). Bulkhead locations and weights are listed in Table 3.

Two watertight bulkheads (fwd and aft) divide the SST into three compartments (Ref. Fig. 7). As shown in Fig. 12, these bulkheads are subjected to internal hydrostatic pressure. Therefore, fwd and aft

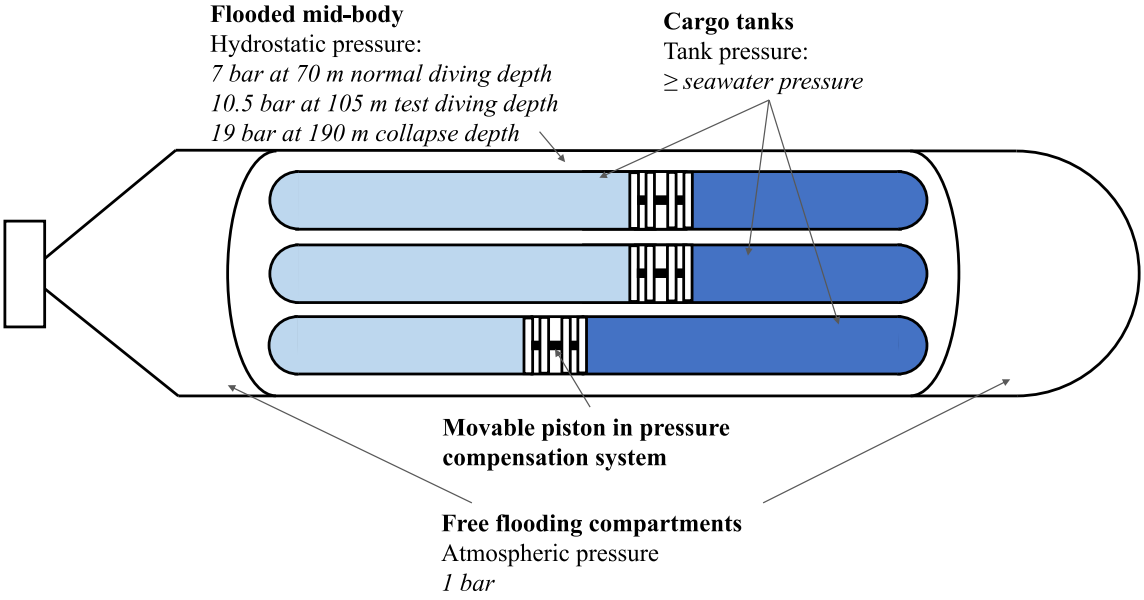

Fig. 12. SST double hull design and forces on external hull and cargo tanks.

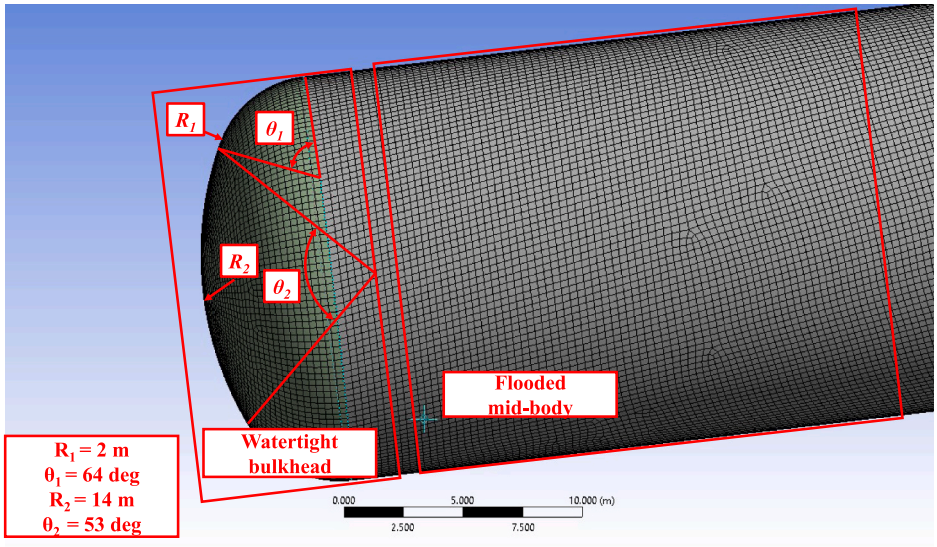

Fig. 13. SST fwd (aft) ellipsoidal watertight bulkhead geometry definition.

bulkheads are pressure vessel heads which are designed against burst pressure. The bulkhead geometry definition is shown in Fig. 13. They employ 53 mm thick VL D37 steel plates. Similarly, for the external hull, the fwd and aft bulkheads are also checked against nominal diving pressure, test diving pressure, and collapse pressure. Appendix C presents the watertight bulkhead finite element analysis result.

The non-watertight bulkheads are not subjected to hydrostatic pressures. Their main function is to provide support to the internal cargo tanks and buoyancy tubes. They are designed to be made of 25 mm steel plates with penetrations to allow the cargo tanks and buoyancy tubes to go through. Similarly, VL D37 steel is applied in the non-watertight bulkheads.

7.2. Internal tank structures

All internal tanks are designed in accordance with ASME BVPC Sec. VIII-2, Chapter 4.3 – Design rules for shells under internal pressure and Chapter 4.4 – Design of shells under external pressure and allowable compressive stresses (ASME, 2015b). It is a requirement that since ASME BPVC is used, the pressure vessel material must be also listed in ASME BPVC Sec. II (ASME, 2015a). SA-738 Grade B is chosen as the pressure vessel material. It is a high strength carbon steel widely used in welded pressure vessels subjected to moderate or lower temperatures. It can be easily provided by many manufacturers like JFE Steel (2021). Details of the design calculations are presented in Appendix D. There are five types of internal pressure vessels in the SST as presented in the general arrangement drawing as illustrated in Fig. 7, i.e., main cargo tank, auxiliary cargo tank, buoyancy tube, compensation tank, and trim tank. The properties of the internal tanks are presented in Table 9 and are also discussed as follows.

7.2.1. Cargo tanks

7.2.1.1. Tank properties. There are 13 cylindrical cargo tanks (seven main and six auxiliary) with hemispherical ends which are circular-symmetrically distributed in the SST's flooded mid-body. The diameters of the main and auxiliary tanks are 5 m and 2.5 m, respectively. The different diameters allow for a more optimal arrangement of the tanks within the SST, thereby maximising space utilisation and consequently payload. These tanks are used for CO_2 storage and have a design burst pressure of 55 bar. This is identified as the worst-case scenario which occurs when the SST is floating on the sea surface. Under this condition, the external hydrostatic pressure is 0 bar gauge, and the pressure difference is 55 bar. The resulting thickness of the main cargo and auxiliary cargo tank cylindrical shells are 57 mm and 29 mm, respectively.

Table 9
SST internal tank properties.

Parameter	Main cargo tank	Auxiliary cargo tank	Compensation tank	Trim tank	Buoyancy tube
Number of tanks	7	6	2	2	8
Length [m]	100	97.5	15	5	100
Diameter [m]	5	2.5	8	7	1.25
Cylinder wall thickness [m]	0.057	0.029	0.015	0.015	0.015
Hemisphere head wall thickness	0.029	0.015	–	–	–
Total volume [m^3]	13,515	2847	1600	400	1030
Steel weight [ton]	4′,769	1026	200	70	368
Material type	SA-738 Grade B	SA-738 Grade B	SA-738 Grade B	SA-738 Grade B	SA-738 Grade B
Material allowable stress [MPa]	244	244	244	244	244
Yield strength [MPa]	414	414	414	414	414
Tensile strength [MPa]	586	586	586	586	586
Allowable burst pressure [bar]	55	55	8	10	29
Allowable collapse pressure [bar]	2.6	2.6	0.7	0.6	7
Design pressure type	Burst	Burst	Burst	Burst	Collapse
Burst pressure UF [-]	2.4	2.4	2.4	2.4	2.4
Collapse pressure UF [-]	2.4	2.4	2.4	2.4	2.4

7.2.1.2. Burst pressure design. The cargo tanks avoid collapse pressure design by utilising a pressure compensation system (PCS) (Ref. Section 9). As illustrated in Fig. 12, cargo tanks are subjected to external hydrostatic pressure and internal tank pressure. Table 10 quantifies these two pressures during normal operating, emergency, and accidental scenarios. It is also noticed that the PCS ensures deterministically that the cargo tank pressure is always greater than the hydrostatic pressure, i.e., the pressure difference will not be negative as presented in Table 10. Details of the PCS system are presented in Section 9.

7.2.2. Compensation tanks and trim tanks

The definition of compensation tanks and trim tanks are given in Section 5.2 They are soft tanks in the free flooding compartments, i.e., they do not need to handle external pressure. Consequently, they only need to handle internal pressure which result from the hydrostatic pressure due to the flooding of the mid-section in the SST. During the calculation, compensation tanks and trim tanks are assumed to be cylindrical to obtain reasonable weight and volume sizing. They can however be made of various shapes to better utilise the space in the free flooding compartments.

7.2.3. Buoyancy tanks

Eight 1.25 m diameter empty buoyancy tanks are arranged at the upper part of the SST to make the vessel neutral buoyant. These buoyancy tanks are 100 m long and are directly connected to the fwd and aft bulkheads, as shown in Fig. 7 Subview B, C, and D. Since these tanks are free flooding, i.e., it is not exposed to water, moisture sensitive equipment can be arranged inside.

The buoyancy tubes are supported along its length. Their unsupported length is set to be 4 m which corresponds to twice of the flooded mid-body frame spacing. These tanks are designed to handle 7 bar hydrostatic pressure corresponds to the 70 m nominal diving depth. The resulting thickness of the buoyancy tubes is 15 mm.

8. Hydrodynamics and propulsion

8.1. Resistance and propulsive power

In general, the SST will travel at a slow speed to minimise resistance to give maximal energy efficiency. The resistance and required propulsive power are 82 kN and 253 kW, respectively, when travelling at an operating speed of 6 knots. Resistance and corresponding propulsive power values are plotted against operating speed and presented in Fig. 14. These values are calculated based on the skin friction obtained from the ITTC-57 correlation line (ITTC, 2011) and the drag pressure obtained empirically from Hoerner (1965). These values increase exponentially with operating speed, i.e., speed is expensive for the SST. Details of the calculations of these values are presented in Appendix B.

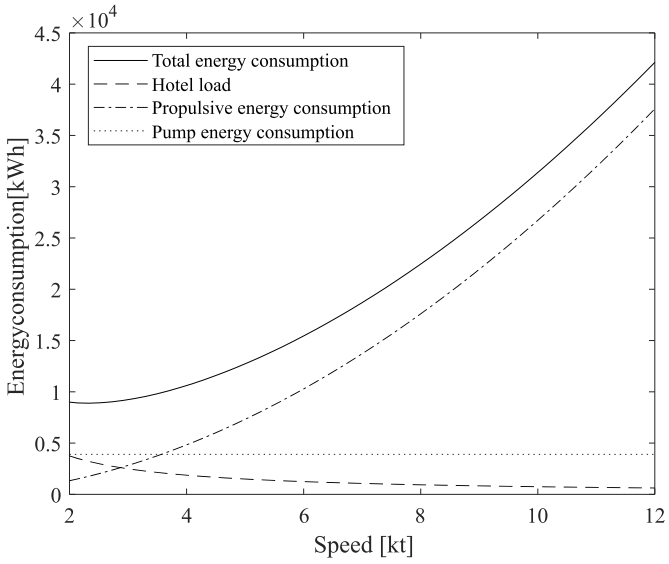

Fig. 14. SST energy consumption to travel 400 km.

The skin friction drag at the hull normally increases with the length of deployed time due to fouling. Widely applied measures to deal with fouling include applying anti-fouling paint and hull cleaning during regular maintenance.

8.2. Propeller

The SST uses the three-bladed Wageningen B-series (Barnitsas et al., 1981) propeller. The propeller has a large diameter of 7 m, a small blade area ratio of 0.3 and a slow operating rotational speed of 38 RPM which provide it a high quasi-propulsive coefficient (QPC) of 0.97. In general, large, slow-rotating, single-screw submarine propellers have high efficiencies (Xing et al., 2021) and the corresponding QPCs are between 0.8 and 1.0. (Renilson, 2015). The thrust and torque coefficients are 0.17 and 0.010, respectively. Other key design parameters are presented in Table 11 with the calculation details presented in Appendix E.

8.3. Propulsion efficiency

The propulsion efficiency is estimated to be 88% using the following expression:

Table 10
Pressure conditions. Emergency ascent (descent) are the recoverable emergency cases when the SST has to ascent (descent). PCS initiate depth is a depth where the hydrostatic pressure exceeds the liquid CO_2 pressure and PCS start functioning. Accidental case is when the SST descents exceed its collapse depth and sinking might happen.

Depth [m]	Cargo	Season	Temperature [°C]	Tank pressure [bar]	Hydrostatic pressure [bar]	Pressure difference [bar]	PCS used	Note
0	CO_2	Summer	20	55.0	0.0	55.0	No	Operating (Surfaced)
		Winter	0	34.9	0.0	34.9	No	
	Water	–	–	0.0	0.0	0.0	Yes	
40	CO_2	Summer	15	50.9	4.0	46.9	No	Uncontrolled ascent
	Water	–	–	4.0	4.0	0.0	Yes	
70	CO_2	Summer	10	45.0	7.0	38.0	No	Operating (Submerged)
		Winter	1	35.8	7.0	28.8	No	
	Water	–	–	7.0	7.0	0.0	Yes	
175	CO_2	Winter	1	35.8	17.5	18.3	No	Uncontrolled descent (Collapse depth)
>358	CO_2	Winter	1	>35.8	>35.8	0.0	Yes	Uncontrolled descent (Accidental case)

Table 11
Propeller parameters.

Parameter	Symbol	Value	Unit
Prop. diameter	D_p	7	[m]
Number of blades	N	3	[-]
Prop/hull ratio	P/H	0.4118	[-]
Propeller pitch/diameter	P/D	0.8	[-]
Tailcone angle	α_c	37.56	[ ]
Propeller speed	n	38	[RPM]
Advance velocity	V_A	2.66	[m/s]
Wake fraction	w_T	0.4722	[-]
Thrust deduction	t	0.1518	[-]
Advance number	J	0.37	[-]
Thrust coefficient	K_T	0.17	[-]
Torque coefficient	K_Q	0.010	[-]
Open water efficiency	η_O	0.60	[-]
Hull efficiency	η_H	1.61	[-]
Relative rotative efficiency	η_R	1.05	[-]
Quasi-propulsive coefficient	QPC	0.97	[-]

$$\eta_p = QPC \cdot \eta_M \cdot \eta_G \tag{1}$$

where η_M and η_G are the motor and gearbox efficiencies, respectively. η_M and η_G are defined to be 94% and 96%, respectively. These are typical values that are common for most electrical drives and gearboxes; examples of these include the ABB IE2 motor and corresponding gearbox which is used in as a ship azimuth thrustor (Hoyer Motor, 2021 and Rolls-Royce, 2021). The calculations lead to a design which provides 289-kW propulsive power at 6 knot speed.

8.4. Hotel load

The SST's hotel load is the power consumption of all systems other than propulsion and pumps. During the trip, the SST's hotel load mainly includes its control units, sensors, and navigation system. This is estimated based on the typical hotel load to propulsion ratio found in today's ships. Wartsila LR2 product tanker and MUNIN reference container ship are used as the reference ships and their hotel load to propulsion power ratios are about 20% (Wärtsilä, 2021a, Kretschmann et al., 2017 and Mau, 2013). In addition, the reduction in power consumption due to the SST being an autonomous vessel, i.e., no crew support systems are considered. This reduction is 40% (Kreschmann, 2017). The propulsive power at the operating speed of 6 knots is 289 kW (Ref. Section 8.3). Therefore, the estimated hotel load is 35 kW:

$$\begin{aligned}&(\text{propulsive power}) \times \tfrac{(\text{hotel load})}{(\text{propulsive power})} \times (\text{auto. reduction})\\ &= 289\ kw \times 0.2 \times 0.6\\ &= 35\ kw\end{aligned} \tag{2}$$

8.5. Pump energy consumption

Cargo pumps and ballast pumps used during the loading and offloading process are another important load on the SST. The pump energy consumption is calculated as follows. The SST allows two load cycles in each trip (load at the port and offload at the well). The energy consumption of each cycle is equal. Each time the SST takes 4 h to load and offload. Pump efficiency is conservatively estimated to be 75% in accordance with Elsey (2020) and Chapter 8 in Hall (2017), which give the efficiency range of large centrifugal pumps and centrifugal compressors, respectively. The cargo pumps can provide 3 bar pressure at a flow rate of 4000 m^3/h. The compensation tank ballast pumps provide 3 bar pressure at a flow rate of 400 m^3/h to compensate for the weight change when loading and offloading. The estimated total loading and offloading energy consumption is 3911 kWh and is calculated using the following equation:

$$\begin{aligned}&\frac{\begin{array}{c}(\text{time}) \times (\text{load cycle}) \times\\ (\text{flow} \times \text{differential pressure})_{cargo} + (\text{flow} \times \text{differential pressure})_{ballast}\end{array}}{3.6 \times 10^6 \times (\text{pump efficiency})}\\ &= 4\ h \times 2 \times \frac{\left(4000\ m^3/h \times 3 \times 10^5 Pa\right) + \left(400\ m^3/h \times 3 \times 10^5 Pa\right)}{3.6 \times 10^6 \times 75\ \%}\\ &= 3.91 \times 10^3\ kWh\end{aligned} \tag{3}$$

8.6. Total energy consumption

The total energy consumption at the operating speed of 6 knots is the sum of the hotel load and propulsion power which gives 324 kW. The pump energy consumption is fixed to be 3911 kWh. This gives a total energy consumption of 15,527 kWh for a range of 400 km (Ref. power consumption plot presented in Fig. 14). For reference, the WSD50 30K LNG carrier (Wärtsilä, 2021b) which is a similar sized 15,000 DWT vessel would consume 160,827 kWh to sail the same voyage, i.e., the SST's energy consumption is of an order of magnitude lower than conventional ships. The low energy consumption enables SST to be fully electrically propelled and therefore emission-free.

8.7. Battery

The SST battery properties are listed in Table 12. The Li-ion battery is chosen for the SST for its high energy density, high specific energy, steady power output, and long service time. Li-ion batteries were first utilised in Japanese Soryu class submarines (Depetro, 2017) and companies like Saab (which is a major submarine manufacturer) are also looking into this technology (Wikström, 2019). The SST is projected to be built within the next decade and since it is expected that technological developments within Li-ion batteries will increase its energy density significantly. It is reasonable to calculate the weight of the battery required using forecasts. The Sion Power 2022 forecast (Mikhaylik et al., 2018) is used and predicts that the specific energy is predicted to be 500 Wh/kg which is about 2.5 times the current typical specific energy of 250 Wh/kg. Based on the forecasted specific energy and a 20% margin, the total battery capacity is 20,000 kWh. As a result, the battery weight of SST is estimated to be 40 tonnes and as previously mentioned, it will be mounted at the aft. The SST can be charged at the port and subsea well during loading and offloading, respectively. The charging time would be in the range of 10 h if a 2000-kW class charger is used. The battery has a life of 1000 discharge cycles or about 8.3 years if two 400 km trips are performed weekly.

8.8. Control appendages and directional stabilities

The SST has six control appendages for manoeuvring. These are two fore hydroplanes, two aft hydroplanes, and two aft rudders. Table 13 lists the directional stability calculation inputs and results when SST is travelling at 6 knots. The calculation process is presented in Appendix F. The horizontal stability index and vertical stability index are 0.37 and 0.77, respectively. These values are within the recommended acceptable ranges listed in Renilson (2015), which are 0.2–0.4 for horizontal stability index and 0.4 to 0.8 for vertical stability index. At this speed, SST's neutral point and critical point locate at (10.1, 0, 0) and (−27.7, 0, 0),

Table 12
Battery pack properties.

Parameter	Value
Specific energy [Wh/kg]	500
Energy density [Wh/l]	1000
Capacity [kWh]	20,000
Weight [t]	40
Volume [m^3]	20
Life cycle	1000 discharge cycles 8.3 years

Table 13
Hydrodynamic coefficients and directional stability indexes @ 6 knots.

SST Hydrodynamic coefficient					
Hydrodynamic coefficient	Value (Hull)				Value (Hull + hydroplanes)
Y_v'	0				−9.6e-2
Y_r'	0				3.8e-2
Z_w'	0				−5.1e-2
Z_q'	0				−3.7e-3
M_w'	−6.2e-4				3.1e-3
M_q'	0				−2.8e-3
N_v'	6.2e-4				3.8e-2
N_r'	0				−1.5e-2
Appendage calculation input					
Hydroplane	**Amount**	**Longitudinal position**	**Slope of lift coefficient $C_{L\alpha}$**	**Drag coefficient C_D**	**Plane area**
Fore hydroplane (vertical motion)	2	30 m	6.1	0.00487	30 m^2
Aft hydroplane (vertical motion)	2	−65 m	2.1	0.015	20 m^2
Rudder (horizontal motion)	2	−65 m	6.1	0.00487	70 m^2
Stability check					
Parameter		**Value**		**Recommended value**	
Horizontal stability index		0.37		0.2–0.4	
Vertical stability index		0.77		0.4–0.8	
Neutral point		(10.1 m, 0 m, 0 m)		-	
Critical point		(-27.7 m, 0 m,0 m)		-	

Table 14
SST vertical stability with respect to different speed.

SST speed (knots)	Vertical stability index	Neutral point x coordinate	Critical point x coordinate	Comments
2	0.48	6.1	−1016.2	Ballast tank or vertical thruster
4	0.65	9.1	−118.7	Fore hydroplanes only
6	0.77	10.1	−27.7	Fore and aft hydroplanes
8	0.84	10.7	−5.3	

respectively. These two points change with the sailing speed and influence the vertical stability. The effect of sailing speed on the vertical stability is presented in Table 14 and described as follows. When the SST is travelling at a moderate speed (6 knots and 8 knots in Table 14), the critical point locates in front of the aft hydroplanes. In these scenarios, SST can use either front or aft hydroplanes for depth control. When its speed reduces, the critical point moves towards the aft and may even be behind the aft hydroplane (4 knots). In these scenarios, using aft hydroplanes for depth control will have no or even negative effects. Thus, only the fore hydroplanes are used for depth control at low speeds as they are located closer to the neutral point and therefore have more effect on heave. However, when the SST is hovering or travelling at very low speed (2 knots or less), the hydroplanes cannot generate adequate lift force for depth changing. In these scenarios, ballast tanks or vertical thrusters should be used.

9. Pressure compensation system

The pressure compensation system (PCS) consists of a movable piston with seals inside the cargo tank separating the CO_2 and seawater. The PCS is illustrated in Fig. 15. The piston seals can be manufactured from polyurethane like those used for batching pigs in pipelines. The pistons can also be equipped with intelligent pigging sensors to monitor important data like tank pressure, cargo temperature, and corrosion status.

The PCS ensures that the internal pressure in the cargo tanks will be always higher or equal to the external pressure (Ref. Table 10). It does this by performing pressure compensations in the following manners.

9.1. Normal operating case

The normal operating case (70 m, summer, liquid CO_2 in Table 10) is presented Fig. 15 (a). As discussed in Section 4.1, CO_2 is transported at 35–55 bar depending on the sea water temperature which varies from 0 to 20 °C. For example, for a seawater temperature of 10 °C, CO_2 will be transported at 45 bar. Some seawater is filled up at the other end of the cargo tanks to fill up the remaining void. The valve is closed and the pressure from the CO_2 will push against the piston which will then react against the sea water; its pressure would be also at 45 bar. The pressure compensation system equalises the pressures of CO_2 and sea water inside the tanks. The operating depth is 70 m, i.e., the external hydrostatic pressure is 7 bar. In this case, the differential burst pressure loading is 38 bar.

9.2. Uncontrolled descent case

As shown in Fig. 15 (b), in an accidental uncontrolled descent case (depth >358 m in Table 10) where the SST descents to a water depth of 500 m, the external hydrostatic pressure will increase to 50 bar. The external pressure is now larger than the internal pressure in the cargo tank by 5 bar. A valve at one end of the cargo tank will open to allow seawater to flow in. The sea water will push against a piston which separates it from the CO_2, thereby also pushing on the CO_2. The internal pressure is therefore equalised to the external pressure and the pressure differential acting on the cargo tank is eliminated. It can ensure the cargo tanks' integrity and avoid leakage in a nonrecoverable accident when the SST sinks.

9.3. Uncontrolled ascent case

Fig. 15 (c) presents an uncontrolled ascent case where the SST ascent to a water depth of 40 m, the external hydrostatic pressure will reduce to 4 bar. Due to the increase of temperature, the CO_2 pressure increases from 45.0 bar to 50.9 bar. The valve is closed and the pressure from the CO_2 will push against the piston towards the seawater. Therefore, the seawater pressure would also increase to 50.9 bar. In this case, the differential burst pressure loading is 46.9 bar.

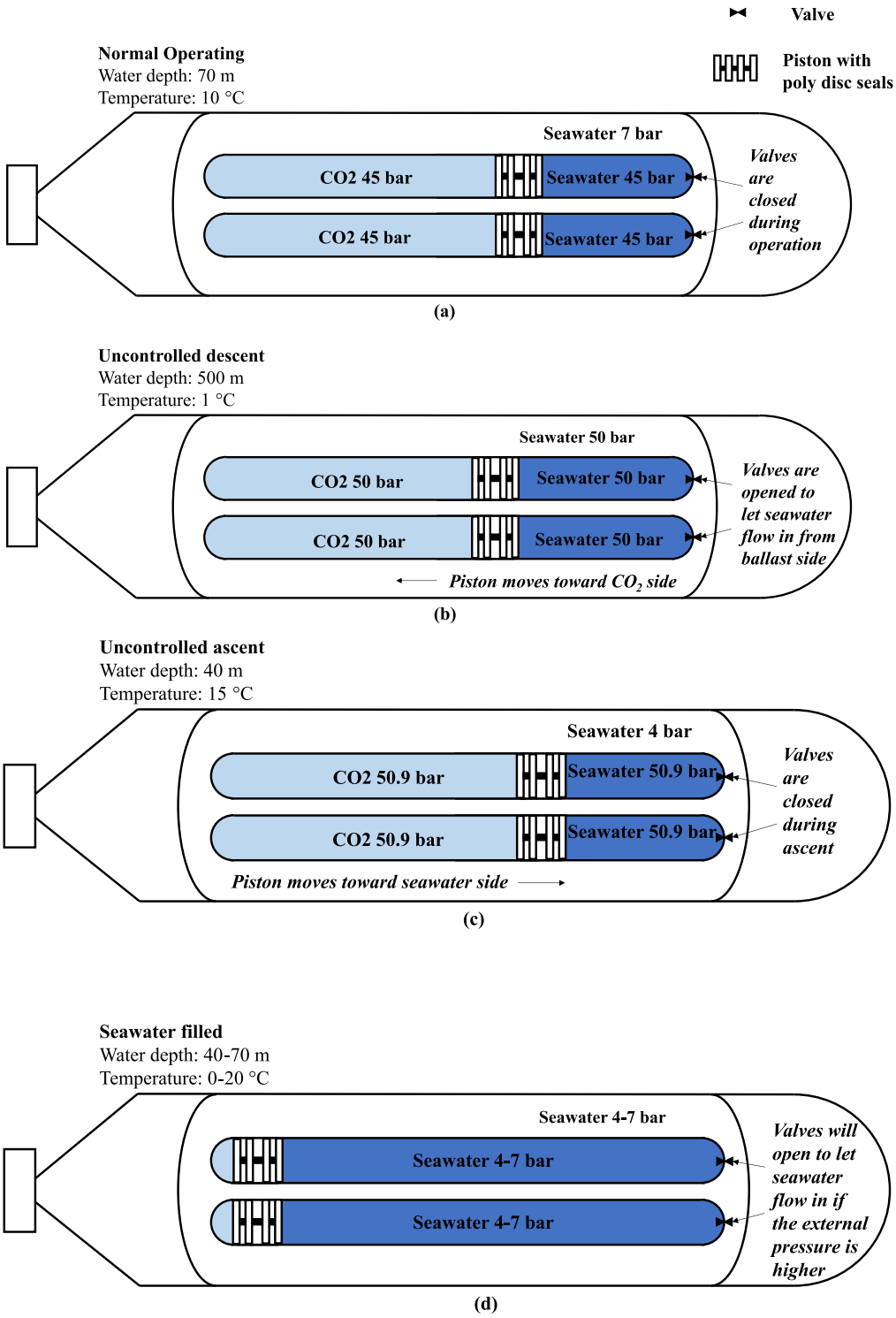

Fig. 15. Pressure compensation system.

9.4. Seawater filled cases

As illustrated in Fig. 15 (d), the seawater filled cases are the situations where the cargo tanks are totally filled with seawater. These happen after the SST is offloaded at a subsea well. In these cases, the tank pressure and external pressure are both hydrostatic pressure (4 bar–7 bar during operation). If the SST changes to a deeper depth, the valves will open and let the seawater flow in to increase the internal pressure until it is equalised to external pressure. Therefore, the external pressure will always lower or equal to internal tank pressure. This allows the cargo tanks to avoid designing for the full external hydrostatic pressure which can be structurally costly.

10. Offloading

The SST will offload CO_2 through a flexible flowline connected to the subsea well while hovering at operating depth in the vicinity. This flowline will be connected to the SST using an ROV. The offloading process is described in the following steps and illustrated in Fig. 16:

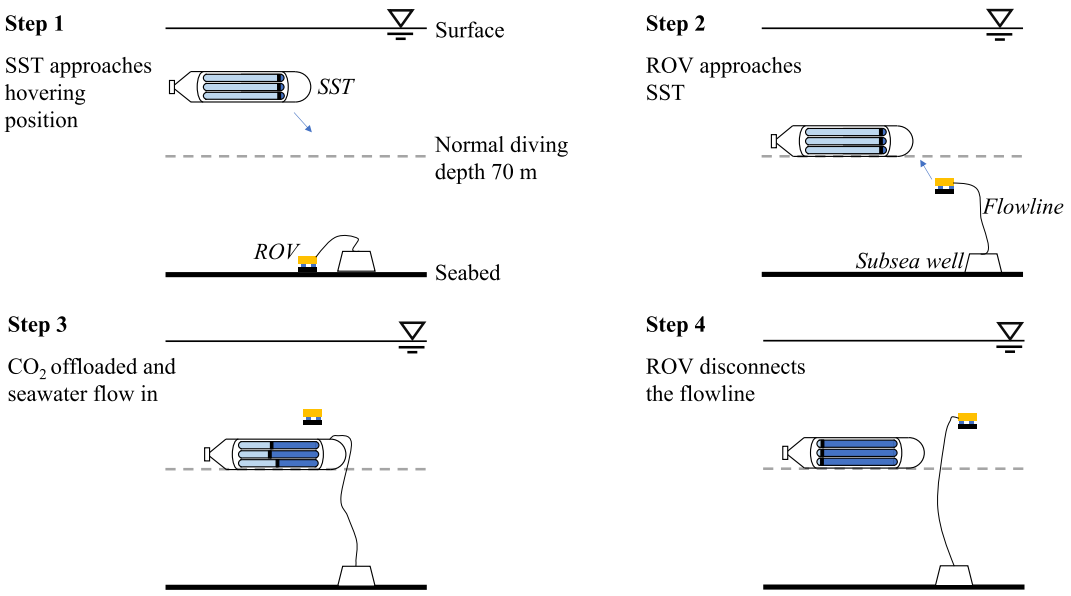

Fig. 16. Offloading method.

- **Step 1:** The SST approaches the subsea well and hovers at operating depth in the vicinity above it.
- **Step 2:** An ROV carries the flowline from the subsea well and flies up to the SST for mating.
- **Step 3:** Liquid CO_2 is pumped out from one end of each cargo tank through the mated connection to the subsea well. Meanwhile, seawater is pumped in from the other end of each cargo tank to fill the void left by the CO_2 and to maintain the tank pressure. The compensation and trim tanks are also used to maintain the SST's trim and neutral buoyancy.
- **Step 4:** The ROV disconnects the flowline after offloading is completed.

This offloading method allows the SST to offload at subsea wells at greater depths while the vessel hovers at a constant operation depth (70 m maximum). Therefore, the SST needs only to be designed for 70 m water depth instead of the subsea wellhead water depth. Besides, this offloading method can also minimise the risk of collision between the SST and subsea facilities since the SST does not need to travel close to the wellhead during the offloading. Additionally, ROV has superior manoeuvrability and would be able to handle the connector and mate it to the SST, even if the SST is moving in the presence of environmental loads.

However, the subsea shuttle tanker still requires a set of dynamic positioning system to maintain its position in currents during the process. According to a CFD analysis performed in Ong and Janocha (2020), the drag force of a side way current is 10 times higher than when the SST is facing current. Therefore, the SST should always face current when it is offloading. The SST's station-keeping analysis requires detailed analysis, but the baseline SST is expected to equip a dynamic positioning system that can limit the maximum displacement within 5 m in a 1 m/s designed current. As an additional reference, Smogeli et al. (2015) performed sea trial and computer model analysis on the station-keeping capability of a 97-m-long platform supply vessel. According to the footprint trajectory obtained, the maximum vessel offsite is around 4 m in a combined wind, wave, and current sea state (wind speed 3 m/s, significant wave height 1m, current speed 0.9 m/s). Therefore, it is reasonable to believe that the SST can deliver the same level of performance.

11. Conclusion

To support research studies into large underwater cargo vehicles, a baseline design of an SST is developed. The purpose of SST is to transport liquid carbon dioxide to subsea wells for direct injection. The SST is proposed to be to an alternative marine transportation method to existing shuttle tankers and subsea pipelines, which may allow the exploration of remote marginal fields as offshore carbon storage sites. The major specifications and features of the SST are provided and include CO_2 properties, hydrostatic properties, structural properties, hydrodynamic properties, pressure compensation system, and offloading method. The SST's main feature is the double hull design with a pressure compensation system which allows the SST to avoid collapse pressure design at the external hull flooded mid-body. This approach helps to reduce the SST's structural weight and contribute to a considerable payload capacity, i.e., 46% of the total displacement. This high payload capacity together with slow service speed allows the SST to maximise its transportation capacity with minimum energy cost.

CRediT authorship contribution statement

Yucong Ma: Conceptualization, Formal analysis, Methodology, Writing – original draft, Writing – review & editing, Visualization. **Yihan Xing:** Conceptualization, Methodology, Supervision, Project administration, Writing – original draft, Writing – review & editing. **Muk Chen Ong:** Conceptualization, Supervision, Investigation, Writing – review & editing. **Tor Henning Hemmingsen:** Investigation, Supervision, Writing – review & editing.

Declaration of competing interest

The authors declare that they have no known competing financial interests or personal relationships that could have appeared to influence the work reported in this paper.

Appendix A. Determination of nominal diving depth

The 70 m nominal diving depth is determined based on minimum recoverable depth from a worst jam-to-rise situation. In this situation, a malfunction in the hydroplane control system is assumed to occur when the SST is sailing at 9.2 knots maximum speed $v_{\max}$ (including 2 knots considering current) speed with a 5° initial pitch angle. After a 5 s reaction time, the SST control system realises the situation and takes restoring reaction. It pumps aft trim tank ballast to the front to decrease the pitch angle. This reduces the ascent speed. The SST can be recovered if the pitch angle is reduced to 0° before reaching the 40 m safety depth.

The following parameters are used in the calculations:

- **Maximum pitch angle:** The maximum pitch angle of the SST is defined to be 5°. The SST does not require an excellent manoeuvrability since it travels constantly at a fixed water depth.
- **Maximum sailing speed:** The maximum sailing speed is defined to be 7.2 knots. This is 20% higher than the SST's design speed.
- **Current:** The designed current speed is set to be 1 m/s (2 knots) at the same speed range with the highest observed current speed of the North Atlantic Current and Norwegian coastal current (Ersdal 2001; Sætre 2007).
- **Trim tank pump capacity:** The maximum trim tank pump capacity is 2000 m^3/h. This can be achieved by two 1000 m^3/h pumps, e.g., Wärtsilä AQ-1200-EC (Wärtsilä 2018).
- **Moment of inertia:** The moment of inertia I_{yy} is estimated to be 7.9e+07 t/m^2 as a solid cylinder using:

$$I_{yy} = \frac{1}{4} W \frac{D^2}{2} + \frac{1}{12} W L^2 \tag{A.1}$$

where W is the SST weight, D is the SST beam, L is the SST length.

- **BG:** The distance of centre of buoyancy and centre of gravity is estimated to be 0.6 m
- **Reaction time:** The reaction time is estimated to be 5 s. Since the SST is autonomous, it has faster response comparing to a normal submarine whose reaction time is around 15 s (Park and Kim, 2018). This is the period before the SST taking recovering reactions after the jam-to-rise happened.

with the above assumptions, the total pitch moment acting on the SST can be calculated as follows:

$$M_{tot} = \underbrace{-L_{trim} \cdot w_{tw}}_{\text{Trim tank restoring moment}} + \underbrace{W \cdot BG \cdot \sin\alpha_{\max}}_{\text{Jammed aft plane}} - \underbrace{\frac{W \cdot BG \cdot \sin\alpha_{\max}}{2}}_{\text{Contribution from the SST CoG}} \tag{A.2}$$

where L_{trim} is the longitudinal distance between two trim tanks, w_{tw} is weight of trim ballast pumped from aft trim tank to fwd trim tank, $\alpha_{\max}$ is the 5° maximum pitch angle.

The pitch angular velocity γ_r is therefore calculated as:

$$\gamma_r = \frac{M_{tot}}{I_{yy}} \tag{A.3}$$

As a result, the recovery time is 60 s, together with the 5 s reaction time, the total ascent time t_{as} is 65 s. The ascent distance is calculated as:

$$d_{as} = v_{max} \cdot \sin \alpha_{max} \cdot t_{as} \tag{A.4}$$

The total ascent distance is calculated to be 26 m. As a result, the lowest recoverable depth in a jam-to-rise situation is 66 m. Base on this, the nominal diving depth is set to be 70 m.

Appendix B. Calculation of resistance forces

This section presents the calculation of resistance forces as a function of slenderness ratio. When the SST is travelling forward, its resistance can be separated into two different components, namely the skin friction and body drag. The skin friction is caused by resistance forces acting on the surface of the body. This means that it is highly dependent on the hull roughness and wetted surface area. The body drag is caused by the pressure difference between the bow and aft of the body which is more dependent on the body shape. The skin friction for a slender structure is normally higher than the body drag because of the high wetted surface area/volume ratio. The resistance components are calculated as following:

The skin friction C_{sf} is derived from the Reynolds number Re in accordance with the ITTC-57 correlation line (ITTC, 2011):

$$C_{sf} = \frac{0.075}{(\log Re - 2)^2} \tag{B.1}$$

A form factor k is introduced to calculate pressure drag C_v contribution using:

$$C_v = (1 + k) C_{sf} \tag{B.2}$$

where k is calculated using the formula from Hoerner (1965). k is expressed as a function of beam D and length L as:

$$k = 1.5 \left(\frac{D}{L}\right)^{\frac{3}{2}} + 7 \left(\frac{D}{L}\right)^3 \tag{B.3}$$

The results are plotted in Fig. 11; the volume is fixed at 32,799 m^3 while the slenderness ratio is varied. This method provides a rough but quick

estimation of the vessel's slenderness in the early stages of the design process. CFD analysis and scaled model tests are usually performed if more accurate results are required.

Appendix C. External hull design calculations

The design calculation method in DNVGL-RU-NAVAL-Pt4Ch1 (DNV-GL, 2018), Appendix A, Section 6 is applied to determine the SST's external hull properties. The calculation input and process are given inTable C 1. The symbols presented in the table are aligned with the notation used in the guideline. The corresponding equation numbers used in the guideline are also mentioned here. The stresses in the free flooding compartments and flooded mid-body external hulls are listed in Table C 2, Table C 3, Table C 4, and Table C 5. The external hulls in free flooding compartments are the pressure hull subjected to hydrostatic pressures. Thus, they are checked against permissible stress at nominal diving depth, test diving depth, and collapse depth in accordance with Chapter 4 in DNVGL-RU-NAVAL-Pt4Ch1 (DNV-GL, 2018). The permissible values are listed in Table C 6. Although the flooded mid-body external hull does not handle hydrostatic pressure, it is designed for 7 bar (70 m) collapse pressure to avoid immediate structural failure in accidental load cases like the malfunction of the mid-body seawater vent.

A finite element analysis is performed to justify the watertight bulkhead design. Table C 7 lists the numerical analysis results and the permissible stresses in DNVGL-RU-NAVAL-Pt4Ch1 Sec.4.3 (DNV-GL, 2018). Fig. C 1 presents the bulkhead equivalent stress distribution under 19 bar collapse depth pressure together with the applied force and boundary condition. Static pressure is applied normal to the ellipsoidal bulkhead from the flooded mid-body. The external hull is clamped at the far end of the mid-body.

Appendix D. Internal tank design calculations

The inner tanks in the SST are designed in accordance with Chapter 4 in ASME BPVC Section VIII, Division 2 (ASME, 2015b). In the SST, main cargo tanks, auxiliary cargo tanks, compensation tanks, and trim tanks are designed to take burst pressure. The buoyancy tubes are designed against collapse pressure.

Tanks under internal pressure

Chapter 4.3.3 and chapter 4.3.5 in ASME VIII-2 (ASME, 2015b) are used to determine the hull thicknesses for the cylindrical shells and hemisphere heads, respectively. The minimum required thickness of a cylindrical hull under internal pressure is expressed as:

$$t_{shell} = \frac{D_t}{2}\left(e^{\frac{p_i}{S_a E_w}} - 1\right) \tag{D.1}$$

where t_{shell} is the hull thickness, D_t is the tank diameter, and S_a is the allowable stress of material. E_w is the weld joint efficiency, this is set to be 1.0 for circumferential joints and longitudinal joints on a shell (Ref. Table 7.2 in ASME VIII-2 (ASME 2015b)). p_i is the design pressure. It is defined to be 55 bar for the cargo tanks and hydrostatic pressure for the trim and composition tanks.

Similarly, the minimum required thickness of a hemisphere heads under internal pressure is expressed as:

$$t_{shell} = \frac{D_t}{2}\left(e^{\frac{0.5 \cdot p_i}{S_a E_w}} - 1\right) \tag{D.2}$$

Tanks under external pressure

Chapter 4.4.5 in ASME VIII-2 (ASME, 2015b) is used to determine the buoyancy tank properties. The step-by-step calculation process can be found in Table D 1.

Appendix E. Propeller characteristics calculations

This appendix presents the calculations used to obtain the propeller characteristics. The propeller open water test data presented in Barnitsas et al. (1981) is used.

Propeller K_T and K_Q and η_O

The wake fraction, w_T, is obtained from Fig. 6.7 in Burcher and Rydill (1994) (reproduced in Fig. D 1) given the tailcone angle, α_c and propeller/hull ratio, P/H.

Inflow velocity advance of the propeller V_A is calculated as:

$$V_A = (1 - w_T)V_s \tag{E.1}$$

The advance number, J is then calculated as:

$$J = \frac{V_A}{nD_p} \tag{E.2}$$

Based on the advance number, J, the thrust and torque coefficients, K_T and K_Q and efficiency, η_O, can be found using the propeller curves from Barnitsas et al. (1981).

Propeller QPC

The thrust deduction, t can be obtained from Fig. 6.8 in Burcher and Rydill (1994) (reproduced in Fig. D 2) given the tailcone angle, α_c and propeller/hull ratio, P/H.

The hull efficiency, η_H, represents the ratio between effective power and thrust power and is calculated as:

$$\eta_H = \frac{1-t}{1-w_T} \tag{E.3}$$

A relative rotative efficiency η_R of 1.05 is used based on the recommendation in Chapter 5.1.5 of Renilson (2015) for similarly sized submarine hulls and propellers. Finally, the quasi-propulsive coefficient (QPC) is calculated as:

$$QPC = \eta_o \cdot \eta_H \cdot \eta_R \tag{E.4}$$

Appendix F. Directional stability calculation

The SST hydrodynamic coefficients are estimated following Section 3.4.3 in Renilson (2015). It is assumed that the SST hull is a spheroid. The equivalent diameter of the spheroid $\overline{d}$ is calculated as:

$$\overline{d} = \left(\frac{6\Delta}{\pi\rho L}\right)^{0.5}$$

The added mass coefficients of a spheroid k_x, k_y, and k_z can then be obtained as:

$$k_y = k_z = -0.00088\left(\frac{L}{\overline{d}}\right)^2 + 0.0245\left(\frac{L}{\overline{d}}\right) + 0.805$$

$$k_x = -0.00047\left(\frac{L}{\overline{d}}\right)^2 + 0.0134\left(\frac{L}{\overline{d}}\right) - 0.059$$

Besides, the nondimensional mass m' is given as:

$$m' = \frac{\Delta}{\frac{1}{2}\rho L^3} \tag{F.2}$$

With above information, the hydrodynamic coefficients of a fore and aft symmetry SST hull in an ideal flow can then be estimated as:

$$\begin{aligned} Y_v' = Y_r' = Z_w' = Z_q' = M_q' = N_r' = 0 \\ M_w' = (k_z + k_x)m' \\ N_v' = -(k_y + k_x)m' \end{aligned} \tag{F.3}$$

where Y, Z, M and N are the force in y-axis (sway), force in z-axis (heave), moment around y-axis (pitch), and moment around z-axis (yaw), respectively. Subscripts v, w q, and r denotes the force is related to velocity in sway, heave, angular velocity in pitch, and angular velocity in yaw, respectively.

After this, the appendages' contribution to the SST hydrodynamic coefficients can be calculated and combined with the hull hydrodynamic coefficients. The appendages' coefficients are calculated following Section 3.4.3.3 in Renilson (2015) and listed in Table 13.

When the hydrodynamic coefficients are determined, the vertical stability index (G_v) can be calculated as:

$$G_v = 1 - \frac{M_w'\left(m' + Z_q'\right)}{M_q' Z_w'} \tag{F.4}$$

Similarly, the horizontal stability index G_h is expressed as:

$$G_h = 1 + \frac{N_v'\left(m' - Y_r'\right)}{N_r' Y_v'} \tag{F.5}$$

Meanwhile, the SST's neutral point x coordinate x_{NP} at small trimming angle and critical point x coordinate x_{CP} are calculated by Eqn F.6 and Eqn F.7, respectively:

$$x_{NP} = -\frac{M_w'}{Z_w'}L \tag{F.6}$$

$$x_{CP} = -\frac{2mgBG}{\rho L^2 Z_w' u^2} - L\frac{M_W'}{Z_W'} \tag{F.7}$$

The directional stability calculation results are listed in Table 13.

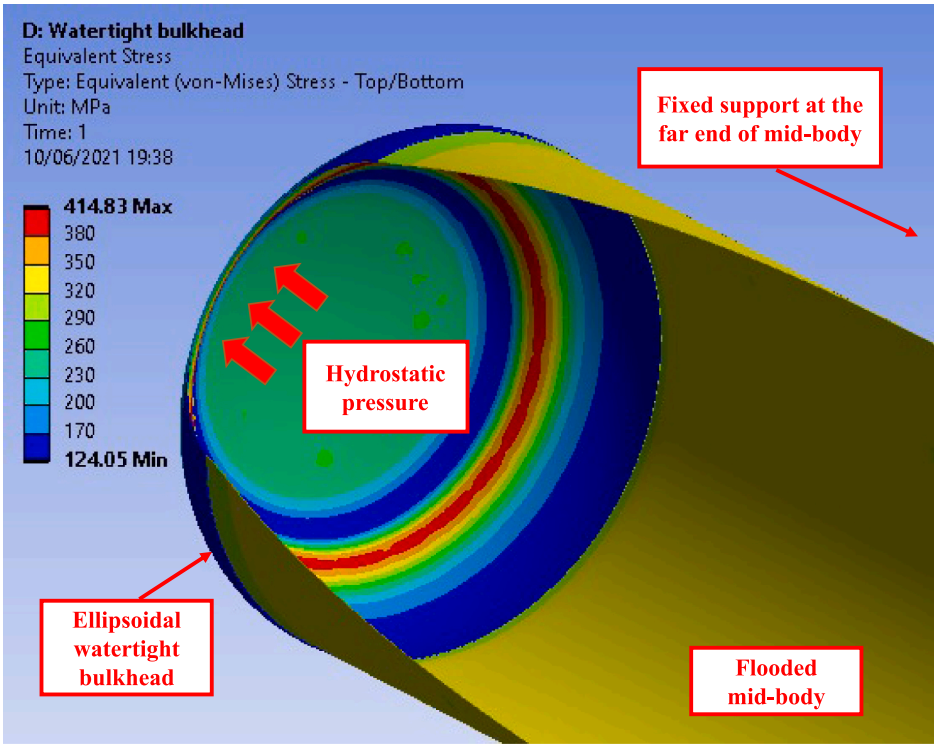

Fig. C. 1. SST bulkhead finite element analysis result at 190 m collapse depth. Hydrostatic pressure is applied inside the flooded mid-body normal to the bulkhead. Fixed support is set at the far end of the mid-body.

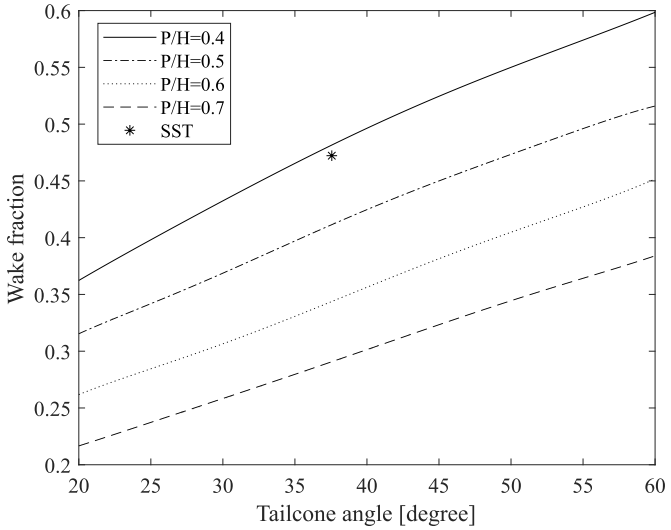

Fig. D. 1. Effects of tailcone angle on wake fraction reproduced from Burcher and Rydill, (1994).

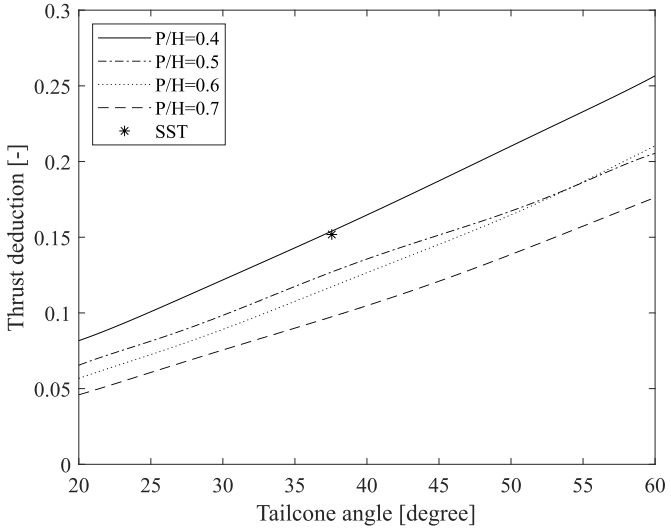

Fig. D. 2. Effects of tailcone angle on thrust deduction reproduced from Burcher and Rydill (1994).

Tab. C. 1
External hull calculation-Collapse diving pressure.

Parameter	Symbol	Free flooding compartment			Flooded compartment	Eq. number in DNVGL RU P4C1 Appendix A
Design pressure type		Nominal diving depth	Test diving depth	Collapse depth	Collapse	
Design pressure	p	7 bar	10.5 bar	19 bar	7 bar	User input
Hull thickness	s	0.041 m	0.041 m	0.041 m	0.025 m	User input
Hull radius	R_m	8.500 m	8.500 m	8.500 m	8.500 m	User input
Frame web height	h_w	0.300 m	0.300 m	0.300 m	0.300 m	User input
Frame web thickness	s_w	0.030 m	0.030 m	0.030 m	0.030 m	User input
Flange width	b_f	0.100 m	0.100 m	0.100 m	0.100 m	User input
Flange thickness	s_f	0.033 m	0.033 m	0.033 m	0.033 m	User input
Frame spacing	L_F	1.000 m	1.000 m	1.000 m	1.500 m	User input
Frame cross sectional area	A_F	0.012 m^2	0.012 m^2	0.012 m^2	0.012 m^2	User input
Inner radius to the flange of frame	R_f	8.15 m	8.15 m	8.15 m	8.15 m	User input
Youngs modulus	E	206 GPa	206 GPa	206 GPa	206 GPa	User input
Poisson Ratio	ν	0.3	0.3	0.3	0.3	User input
Poisson ratio in elastic-plastic range	ν_p	0.300	0.300	0.309	0.300	(A48)
Frame distance without thickness	L	0.97 m	0.97 m	0.97 m	1.47 m	(A9)
Effective length	L_{eff}	0.91 m	0.91 m	0.91 m	0.72 m	(A10)
Effective area	A_{eff}	0.013 m^2	0.013 m^2	0.013 m^2	0.013 m^2	(A11)
The radial displacement in the middle between the frames	w_M	−0.0035 m	−0.0053 m	−0.0093 m	−0.0087 m	(A15)
The radial displacement at the frames	w_F	−0.0019 m	−0.0027 m	−0.0057 m	−0.0094 m	(A16)
The reference stress is the circumferential stress in the unstiffened cylindrical pressure hull	σ_o	145 MPa	218 MPa	394 MPa	238 MPa	(A13)
The equivalent stresses are composed of the single stresses in longitudinal and circumferential direction at the middle between frames	$\sigma^m{}_{v,m}$	95 MPa	142 MPa	252 MPa	214 MPa	(A14)
The equivalent stresses are composed of the single stresses in longitudinal and circumferential direction at the frames	$\sigma^m{}_{v,f}$	70 MPa	104 MPa	197 MPa	236 MPa	(A14)
Average membrane stress in longitudinal direction	$\sigma^m{}_x$	73 MPa	109 MPa	197 MPa	119 MPa	(A17)
Membrane stress in circumferential direction in the middle between the frames	$\sigma^m{}_{\phi,M}$	108 MPa	160 MPa	284 MPa	247 MPa	(A18)
Membrane stress in circumferential direction at the frames	$\sigma^m{}_{\phi,F}$	67 MPa	98 MPa	197 MPa	272 MPa	(A19)
Bending stresses in longitudinal direction in the middle between the frames	$\sigma^x{}_{\phi,M}$	28 MPa	45 MPa	93 Mpa	126 MPa	(A20)
Bending stresses in longitudinal direction at the frames	$\sigma^b{}_{x,F}$	95 MPa	149 MPa	255 MPa	69 MPa	(A21)
Bending stresses in circumferential direction in the middle between the frames	$\sigma^b{}_{\phi,M}$	8 MPa	13 MPa	28 MPa	38 MPa	(A22)
Bending stresses in circumferential direction at the frames	$\sigma^b{}_{\phi,F}$	29 MPa	45 MPa	76 MPa	21 MPa	(A23)
Tangential module	E_t	206 GPa	206 GPa	206 GPa	206 GPa	(A38)
Secant module	E_s	206 GPa	206 GPa	199 GPa	206 GPa	(A39)
Elastic buckling pressure	$p^{el}{}_{cr}$	58.3 bar	58.3 bar	58.3 bar	39.9 bar	(A21)
Theoretical elastic-plastic buckling pressure	$p^{i}{}_{cr}$	57.0 bar	57.0 bar	57.0 bar	39.9 bar	(A22)
Reduction factor	r	0.75	0.75	0.75	0.75	(A23)
Elastic-plastic buckling pressure	p'_{cr}	42.9 bar	42.9 bar	42.9 bar	39.9 bar	(A23)•(A23)

Tab. C. 2
Stresses in the free flooding compartment (normal diving depth).

Types of stresses	At the frame			In the middle of the field		
	Circumferential	Equivalent	Axial	Circumferential	Equivalent	Axial
Membrane stress [MPa]	67	-	73	108	-	73
Membrane equivalent stress [MPa]	-	95	-	-	70	-
Bending stresses [MPa]	29	-	95	8	-	28
Normal stress outside [MPa]	96	-	168	116	-	101
Equivalent normal stress outside [MPa]	-	146	-	-	109	-
Normal stress inside [MPa]	96	-	168	116	-	101
Equivalent normal stress inside [MPa]	-	146	-	-	109	-

Tab. C. 3
Stresses in the free flooding compartment (test diving depth).

Types of stresses	At the frame			In the middle of the field		
	Circumferential	Equivalent	Axial	Circumferential	Equivalent	Axial
Membrane stress [MPa]	98	-	109	160	-	109
Membrane equivalent stress [MPa]	-	142	-	-	104	
Bending stresses [MPa]	45	-	149	13	-	45
Normal stress outside [MPa]	142	-	257	174	-	153
Equivalent normal stress outside [MPa]	-	223	-	-	164	-
Normal stress inside [MPa]	142	-	257	174	-	153
Equivalent normal stress inside [MPa]	-	223	-	-	164	-

Tab. C. 4
Stresses in the free flooding compartment (collapse depth).

Types of stresses	At the frame			In the middle of the field		
	Circumferential	Equivalent	Axial	Circumferential	Equivalent	Axial
Membrane stress [MPa]	197	-	197	284	-	197
Membrane equivalent stress [MPa]	-	252	-	-	197	-
Bending stresses [MPa]	76	-	255	28	-	93
Normal stress outside [MPa]	273	-	452	312	-	290
Equivalent normal stress outside [MPa]	-	394	-	-	302	-
Normal stress inside [MPa]	273	-	452	312	-	290
Equivalent normal stress inside [MPa]	-	394	-	-	302	-

Tab. C. 5
Stresses in the flooded compartment.

Types of stresses	At the frame			In the middle of the field		
	Circumferential	Equivalent	Axial	Circumferential	Equivalent	Axial
Membrane stress [MPa]	272	-	119	247	-	119
Membrane equivalent stress [MPa]	-	214	-	-	236	-
Bending stresses [MPa]	21	-	69	38	-	126
Normal stress outside [MPa]	293	-	188	285	-	245
Equivalent normal stress outside [MPa]	-	257	-	-	267	-
Normal stress inside [MPa]	293	-	188	285	-	245
Equivalent normal stress inside [MPa]	-	257	-	-	267	-

Tab. C. 6
External hull permissible stresses (Ref. Sec.4.3 in DNV-GL, 2018).

Location (depth)	VL D47 Tensile strength	VL D47 Yield strength	Permissible stress calculation	Permissible stress value	Results
Free flooding compartment (nominal diving depth)	550 MPa	460 MPa	$min\left\{\frac{550\ MPa}{2.7}, \frac{460\ MPa}{1.7}\right\}$	203 MPa	Tab. C2
Free flooding compartment (test diving depth)	550 MPa	460 MPa	$\frac{460\ MPa}{1.1}$	418 MPa	Tab. C3
Free flooding compartment (collapse depth)	550 MPa	460 MPa	$\frac{460\ MPa}{1.0}$	460 MPa	Tab. C4
Flooded compartment (collapse depth)	550 MPa	460 MPa	$\frac{460\ MPa}{1.0}$	460 MPa	Tab. C5

Tab. C. 7
Watertight bulkhead equivalent stresses and permissible stresses.

Case	Depth	Maximum equivalent stress	Permissible stress (Ref. Sec.4.3 in DNVGL RU P4C1)	Criterion fulfilled?
Nominal diving depth	70 m	153 MPa	203 MPa	Yes
Test diving depth	105 m	229 MPa	418 MPa	Yes
Collapse depth	190 m	415 MPa	460 MPa	Yes

Tab. D. 1
Buoyancy tube calculation.

Parameter	Symbol in ASME BPVC Sec. VIII Div.2	Value	Eq. number in ASME BPVC Sec. VIII Div.2
Thickness	t	0.015 m	User input
Outer diameter	D_o	1.28 m	User input
Unsupported length	L	4 m	User input
Young's modulus	E_y	200 GPa	User input
Minimum yield strength	S_y	414 MPa	User input
Design factor	FS	2.4	(4.4.1)
Predicted elastic buckling stress	F_{he}	84 MPa	(4.4.19)
Factor	M_x	41	(4.4.20)
Factor	C_h	0.02	(4.4.22)
Predicted buckling stress	F_{ic}	84 MPa	(4.4.27)
Allowable external pressure	P_a	8 bar	(4.4.28)

References

26th ITTC Resistance Committee, 2011. Recommended Procedures and Guidelines: Resistance Test, International Towing Tank Committee (ITTC) (ITTC). Zürich, Switzerland.

ASME, 2015a. Boiler and Pressure Vessel Code, Section II. Part D, The American Society of Mechanical Engineers, New York, USA.

ASME, 2015b. Boiler and Pressure Vessel Code, Section VIII, Division 2. The American Society of Mechanical Engineers, New York, USA.

Barnitsas, M.M., Ray, D., Kinley, P., 1981. KT, KQ and Efficiency Curves for the Wageningen B-Series Propellers. University of Michigan.

Bonis, M., 2012. Managing the Corrosion Impact of Dense Phase CO2 Injection for an EOR Purpose. Abu Dhabi International Petroleum Conference and Exhibition, Abu Dhabi. UAE, 11 Nov 2012. https://doi.org/10.2118/161207-MS.

Brandt, H., Fruhling, C., Hollung, A., Schiemann, M., Vob, T., 2015. A Multipurpose Submarine Concept for Arctic Offshore Operations, OTC Arctic Technology Conference. OTC-25501-MS, Copenhagen, Denmark. March 2015. https://doi.org/10.4043/25501-MS.

Burcher, R., Rydill, L.J., 1994. Concepts in Submarine Design. Cambridge University Press, Cambridge, UK.

Carbon Capture and Storage Association (CCSA), 2020. What Is CCS?, assessed Sep 2020 from. http://www.ccsassociation.org/what-is-ccs/.

De Visser, E., Hendriks, C., Barrio, M., Mølnvik, M.J., de Koeijer, G., Liljemark, S., Le Gallo, Y., 2008. Dynamis CO2 quality recommendations. International Journal of Greenhouse Gas Control 2 (4), 478–484. https://doi.org/10.1016/j.ijggc.2008.04.006.

Depetro, A., 2017. The Design & Safety Challenges of a Lithium-Ion Main Storage Battery for Conventional Submarines, the 4th SIA Submarine Science, Technology and Engineering Conference.

DNV-GL, 2018. Rules for Classification, Naval Vessels, Part 4 Sub-surface Ships (Chapter 1) Submarines.

DNV-GL, 2019. Rules for Classification, Ships, Part 2 Materials and Welding (Chapter 2) Metallic materials.

Eiken, O., Ringrose, P., Hermanrud, C., Nazarian, B., Torp, T.A., Høier, L., 2011. Lessons learned from 14 years of CCS operations: Sleipner. Salah and Snøhvit, Energy Procedia 4, 5541–5548. https://doi.org/10.1016/j.egypro.2011.02.541.

Ellingsen, K.E., Ravndal, O., Reinas, R., Hansen, J.H., Marra, F., Myhre, E., Dupuy, P.M., Sveberg, K. (2020). RD677082 Subsea Shuttle System.

Elsey, J., 2020. How to Define & Measure Centrifugal Pump Efficiency: Part 1 assessed May 2021 from. https://www.pumpsandsystems.com/how-define-measure-centrifugal-pump-efficiency-part-1#:~:text=Centrifugal%20pumps%20can%20approach%2094,will%20vary%20by%20plant%20type.

Equinor ASA, 2020. Northern Lights CCS assessed Sep 2020 from. https://www.equinor.com/en/what-we-do/northern-lights.html.

Equinor ASA, 2021. EL001 Northern Lights - Receiving and Permanent Storage of CO2 assessed Mar 2021 from. https://northernlightsccs.com/wp-content/uploads/2021/03/RE-PM673-00011-02-Impact-Assessment.pdf.

Equinor Energy AS, 2019. RD662093 Subsea Shuttle System.

Ersdal, G., 2001. An Overview of Ocean Currents with Emphasis on Currents on the Norwegian Continental Shelf. Technical report. Norwegian Petroleum Directorate.

Fullenbaum, R., Fallon, J., Flanagan, B., 2013. Oil & Natural Gas Transportation & Storage Infrastructure: Status, Trends, & Economic Benefits. Technical report. IHS Global Inc. https://www.circleofblue.org/wp-content/uploads/2014/12/API-Infrastructure-Investment-Study.pdf.

Hall, S., 2017. Rules of Thumb for Chemical Engineers. Butterworth-Heinemann, Oxford, UK.

Hoerner, S.F., 1965. Fluid-dynamic Drag: Practical Information on Aerodynamic Drag and Hydrodynamic Resistance. Published by the author. California, USA.

International Energy Agency (IEA), 2010. Energy Technology Perspectives 2010: Scenarios and Strategies to 2050. OECD Publishing, Paris, France.

Jacobsen, L.R., 1971. Subsea Transport of Arctic Oil - A Technical and Economic Evaluation. Offshore Technology Conference, OTC-1425-MS, Houston, TX, USA, 2 May 1971. https://doi.org/10.4043/1425-MS.

Jacobsen, L., Lawrence, K., Hall, K., Canning, P., Gardner, E., 1983. Transportation of LNG from the arctic by commercial submarine. Marine Technology and SNAME News 20 (4), 377–384. https://doi.org/10.5957/mt1.1983.20.4.377.

Kretschmann, L., Burmeister, H.-C., Jahn, C., 2017. Analyzing the economic benefit of unmanned autonomous ships: an exploratory cost-comparison between an autonomous and a conventional bulk carrier. Research in Transportation Business & Management 25, 76–86. https://doi.org/10.1016/j.rtbm.2017.06.002.

Mariano, A., Ryan, E., Perkins, B., Smithers, S., 1995. The Mariano Global Surface Velocity Analysis 1.0. United States Coast Guard Research and Development Centre. Technical report no. CG-D-34-95.

Mau, G., 2013. Handbuch Dieselmotoren im Kraftwerks-und Schiffsbetrieb. Springer-Verlag, Wiesbaden, Germany.

Mikhaylik, Y., Kovalev, I., Scordilis-Kelley, C., Liao, L., Laramie, M., Schoop, U., Kelley, T., 2018. 650 Wh/kg, 1400 Wh/L Rechargeable Batteries for New Era of Electrified Mobility, 2018. NASA Aerospace Battery Workshop, Alabama, USA, 28 November.

Mohitpour, M., Golshan, H., Murray, A., 2007. Pipeline Design & Construction: a Practical Approach. The American Society of Mechanical Engineers, New York, USA.

Motor, Hoyer, 2021. IE2 Marine Motor — 365 kW - 4P. - Frame 355 - B3, assessed Sep 2020 from. https://hoyermotors.com/products/motors/hoyer-ie2-marine-motors/.

National Centers for Environmental Information (NCEI), 2020. Greenland, Iceland andNorwegian Seas Regional Climatology assessed Sep 2020 from. https://www.ncei.noaa.gov/products/greenland-iceland-and-norwegian-seas-regional-climatology.

Norwegian Petroleum Directorate (NPD), 2020. Carbon Capture and Storage assessed Aug 2020 from. http://www.norskpetroleum.no/en/environment-and-technology/carbon-capture-and-storage/.

Ong, M.C., Janocha, M.J., 2020. CFD Analysis of Equinor Subsea Shuttle, Technical Report Delivered to Equinor. University of Stavanger, Stavanger, Norway.

Palmer, A., King, R., 2008. Subsea Pipeline Engineering, second ed. PennWell Corp, Oklahoma, USA.

Papanikolaou, A., 2014. Ship Design: Methodologies of Preliminary Design. Springer, Dordrecht Heidelberg New York London.

Park, J.Y., Kim, N., 2018. Design of a safety operational envelope protection system for a submarine. Ocean. Eng. 148, 602–611. https://doi.org/10.1016/j.oceaneng.2017.11.016.

Renilson, M., 2015. Submarine Hydrodynamics. Springer, Cham, Switzerland.

Rolls-Royce, 2021. Marine Products and Systems assessed Sep 2020 from. https://www.rolls-royce.com/~/media/Files/R/Rolls-Royce/documents/marine-product-finder/MPS%202017%20LR.pdf.

Ross, C.T., 2011. Pressure Vessels: External Pressure Technology, second ed. Woodhead Publishing, Cambridge, UK.
Šabalja, T., Senjanović, I., Hadžić, N., 2014. Structural design of a typhoon class submarine. In: 21st Symposium on Theory and Practice of Shipbuilding with International, 397.
Sætre, R., 2007. The Norwegian Coastal Current: Oceanography and Climate, Fagbokforlaget, Bergen, Norway.
Smogeli, Ø., Nguyen, D.T., Eide, K., Pivano, L., 2015. DynCap—Full Scale Validation of a Vessel's Station-Keeping Capability Analysis. Dynamic Position Conference, Houston, TX, USA. October 2015.
Steel, J.F.E., 2021. Steel Plate, Cat.No.C1E-001-08 assessed May 2021 from. https://www.jfe-steel.co.jp/en/products/plate/catalog/c1e-001.pdf.
Taylor, P., Montgomery, J., 1977. Arctic Submarine Tanker System. Offshore Technology Conference, OTC-2998, Houston, TX, USA, 2 May 1977. https://doi.org/10.4043/2998-MS.
Vestereng, C., 2019. Shuttle Tankers in Brazil assessed Sep 2020 from. https://www.dnv.com/expert-story/maritime-impact/shuttle-tankers-Brazil.html.
Wärtsilä, 2018. Aquarius EC Ballast Water Management System Product Leaflet assessed May 2020 from. https://www.wartsila.com/docs/default-source/product-files/bwms-files/brochure-o-aquarius-ec.pdf?utm_source=bwms&utm_medium=bwms&utm_term=aquariusec&utm_content=brochure&utm_campaign=msleadscoring.
Wärtsilä, 2021a. LR2 Product Tanker Data Sheet assessed Sep 2020 from. https://cdn.wartsila.com/docs/default-source/product-files/sd/merchant/tankers/data-sheet-ship-design-tanker-wsd47-113k.pdf?sfvrsn=c447c545_5.
Wärtsilä, 2021b. WSD50 30K 30,000 M3 LNG Carrier Data Sheet assessed Apr 2021 from. https://cdn.wartsila.com/docs/default-source/product-files/sd/merchant/lng/wsd50-30k-lng-carrier-ship-design-o-data-sheet.pdf?sfvrsn=e8b38445_8.
Wikström, A., 2019. Lithium Ion Battery - Opportunities and Challenges for Submarines, Presentation in 2019 Underwater Defence Technology. Stockholm, Sweden. May 2019.
Wilson, J., 2008. Shuttle tankers vs pipelines in the GOM frontier. World Oil 229 (4), 149–151.
Xing, Y., 2021. A Conceptual Large Autonomous Subsea Freight-Glider for Liquid CO2 Transportation. In: International Conference on Offshore Mechanics and Arctic Engineering, OMAE2021-61924, Virtual, Online, 21 – 30 June 2021.
Xing, Y., Ong, M.C., Hemmingsen, T., Ellingsen, K.E., Reinas, L., 2021. Design considerations of a subsea shuttle tanker system for liquid carbon dioxide transportation. J. Offshore Mech. Arctic Eng. 143 (4), 045001 https://doi.org/10.1115/1.4048926.